How Reactants Polarization Can Be Used to Change and Unravel Chemical Reactivity

Jesús Aldegunde

Departamento de Química Física, Facultad de Ciencias Químicas, Universidad de Salamanca, Salamanca, Spain

Marcelo P. de Miranda* and James M. Haigh

School of Chemistry, University of Leeds, Leeds LS2 9JT, United Kingdom

Brian K. Kendrick

Theoretical Division (T-12, MS-B268), Los Alamos National Laboratory, Los Alamos, New Mexico 87545

V. Sáez-Rábanos

Departamento de Química y Bioquímica, Escuela Técnica Superior de Ingenieros de Montes, Universidad Politécnica de Madrid, 28040 Madrid, Spain

F. Javier Aoiz†

Departamento de Química Física, Facultad de Química, Universidad Complutense, 28040 Madrid, Spain

Received: March 9, 2005; In Final Form: May 10, 2005

This article presents theoretical methods for the description of the directional effect of reactant rotation on the reactivity of atom−diatom systems and suggests an experiment that could be used to test theoretical predictions. The theory can be used in conjunction with both quantum reactive scattering and quasiclassical trajectory calculations, and is stated in general terms, which allows it to deal with arbitrary reactant polarizations. The illustrative results obtained for the benchmark $H + D_2$ reaction are also presented and show that under experimentally achievable conditions one can largely control reactive cross sections and product state distributions, while at the same time gaining valuable and at times surprising information on the reaction mechanism.

1. Introduction

Two of the most persistent goals of scientific investigations of the dynamics of molecular collisions are understanding and control.[1,2] On one hand, collision dynamicists strive for a detailed understanding of collision mechanisms and of the role of energetic and directional factors in scattering events.[3−5] On the other hand, they attempt to devise techniques for the control of molecular collisions and, in particular, for the selection of desired collision outcomes.[6−8] Naturally, the two endeavors go hand in hand. The understanding of collision mechanisms facilitates the development of control schemes, whereas analysis of the dynamics of controlled collisions can offer important clues about collision mechanisms.

The subject matter of this article is related to both issues. We consider here the role of reactant polarization in the dynamics of reactive collisions and present theoretical methods that can be useful (i) for the analysis of the dependence of reaction mechanisms on reactant polarization and (ii) for the selection of optimum reactant polarization schemes for the control of reaction probabilities and product state distributions. To encourage experimental approaches to the problem, we also describe what we consider to be a challenging yet feasible experiment capable of probing the phenomena we address theoretically and include, among other illustrative results, theoretical predictions for possible outcomes of the proposed experiment.

From a purely theoretical point of view, there is no significant difference between reactants and products polarization. What matters in either case is whether the reaction probability changes when the collision partners are polarized, in other words, whether the reaction dynamics privileges certain relative molecular orientations or relative directions of motion. (For articles discussing this and many other aspects of the dependence of reaction dynamics on spatial directions, see the special editions of journals dedicated to the biennial stereodynamics conferences, refs 9−16.)

From a practical point of view, however, there are differences. An important one is that reactant polarization is determined by external intervention (laboratory preparation of polarized reactants), whereas product polarization is determined by the reaction itself. In particular, this means that in practice one cannot fully control the polarization of the reactants with regard to the (body-fixed) collision reference frame.

Another important difference is that common intuition and practical applications generally introduce a bias in the way one regards a chemical reaction: although the state of reactants is seen as a factor that causes the dynamics to unfold the way it does, the formation of products in a particular state is seen as but a consequence of it. It is as if reactants existed a priori and products only a posteriori, even when the application under consideration actually involves a time-independent process. This

* Corresponding author. E-mail: m.miranda@leeds.ac.uk.
† E-mail: aoiz@quim.ucm.es.

10.1021/jp0512208 CCC: $30.25
Published on Web 06/17/2005

makes reactant preparation a much more obvious choice for the control of reaction probabilities than product selection. (Here we are talking about control in the passive sense: external intervention is restricted to the asymptotic conditions of the reactive system. In active control schemes, the external intervention is not restricted in this way.)

Studies of reactant polarization must therefore deal with this dichotomy. The theory is most powerful when the collision is examined from a body-fixed perspective and does not require formal distinctions between reactants and products. Practical applications, however, are at least partially restricted to space-fixed points of view and do introduce distinctions between reactants and products. Instead of developing separate methods appropriate for particular cases, it is convenient to obtain a general method that allows for transformations from general situations to particular cases. This is precisely the approach we have used.

As already mentioned, our main interest here is in the role of reactant polarization in the dynamics of reactive collisions. For the sake of objectivity, our presentation and examples are adapted to this situation. Other situations in which one is interested, say, in both reactant and product polarization, or else in nonreactive as well as reactive collisions, can be dealt with by generalized versions of the methodology presented here.

We present two versions of our method: one classical, appropriate for use in conjunction with quasiclassical trajectory (QCT) calculations, the other quantum mechanical, appropriate for use in conjunction with quantum scattering calculations. In either case, we also consider the procedures (transformations between laboratory and collision reference frames) necessary for the analysis of actual reactant polarization experiments. Illustrative examples, in which we consider the $H + D_2(v = 0, j = 2)$ reaction and possible experiments involving D_2 alignment, are also presented.

The quantum and classical theoretical methods presented here are modified and extended versions of the quantum[17,18] and classical[18,19] methods we have used before for the description of polarization effects in the dynamics of atom−diatom reactions, which in turn were strongly based on previous vector correlation theories.[20−30] We have stated the quantum and classical theories using analogous formalisms and have revised or extended some of the definitions used in the past in order to maximize the chemical insight that can be gained by analysis of the calculable (and observable) quantities and in order to facilitate the comparison between (possibly experimental) quantum and classical results.

The reason for the selection of an example involving reactant alignment at a $j = 2$ rotational level (as opposed to a more general polarization state, also involving the orientation or coherent superposition of states with different rotational quantum numbers) is our belief in the feasibility of experiments of this type involving reactions amenable to accurate theoretical treatment. Indeed, one such experiment has already been performed by Zare and co-workers at Stanford University.[19] They have measured HD alignment effects in the dynamics of the $Cl + HD(v = 1, j = 2)$ reaction using stimulated Raman pumping (SRP) to prepare $HD(v = 1, j = 2, m = 0)$ molecules (quantization axis along the laser polarization direction **E**) by pumping of the $S(0)$ transition with parallel laser polarization. This corresponds to negative alignment of the rotational angular momentum vector (**j** preferentially perpendicular to **E**), and to positive alignment of the HD internuclear axis (**r** preferentially parallel/antiparallel to **E**). The use of different experimental geometries has enabled them to obtain experimental values for the HD alignment moments, and this provided important clues for the analysis of the reaction dynamics, which was also done by considering theoretical results from QCT and quantum scattering calculations[19] on the G3 potential energy surface.[31] Alignment effects were found to be important, with close-to-collinear collisions enhancing reactivity.

We would also like to note that, although the fact that the mutual orientation of reagent molecules influences chemical reactions is rather obvious, much remains to be done if we are to thoroughly understand how exactly and to what extent that is so. Indeed, it is often the case that detailed studies of the stereodynamics of molecular collisions lead to surprising, counterintuitive results. Examples are abundant (see, for instance, refs 9−16), but a particularly striking one is provided by the Li + HF system. Quantum theoretical studies[32,33] of this reaction at zero total angular momentum and with HF in its ground vibrational state have indicated that formation of the LiF product is favored not only when the Li atom attacks the F end of HF, as one would intuitively expect, but also (and perhaps more strongly) when the Li atom attacks the H end of HF, an effect that had also been suggested by early QCT calculations.[34] Experimental studies of the same reaction by Loesch and co-workers,[35,36] this time involving $HF(v = 1)$ molecules, have confirmed steric effects to be important, but in a rather different manner. The detailed analysis of their data was carried out in the light of wave-packet[37] and QCT[38] calculations, and the theoretical studies have lead to the conclusion that steric effects are actually quite unimportant for the integral reaction cross section summed over product states but much more significant for differential properties and for the product state distribution, with formation of LiF in its $v' = 0$ or $v' = 3$ vibrational states being favored, respectively, by head-on or side-on Li + HF collisions.[38]

Detailed stereodynamical studies are therefore important to solidify our understanding of the mechanisms of chemical reactions, and can also point out if and to what extent the selection of reactant states can be used to manipulate reaction probabilities and product state distributions. This paper discusses theoretical and experimental methods that have the potential to be useful in that regard, along with illustrative examples.

The article is organized as follows. The presentation of the theory starts in Section 2 with a description of the quantities involved and their physical meanings, and is concluded in Section 3 with an account of the mathematical and computational procedures necessary for actual calculations. This is followed in Section 4 by the description of the reactant polarization experiment we are proposing. Results that illustrate how the theory can be used, and also what can be observed in the proposed experiment, are presented in Section 5. Section 6 then closes the paper with a summary of our main results and conclusions.

2. Overview of Theory

Every chemical reaction is a transformation. In the case of atom−diatom reactions, it is usual to think about the transformation as being given by

$$A + BC(v, j, m) \xrightarrow{E_{coll}, \theta} AB(v', j', m') + C \qquad (1)$$

where v, j, m and their primed counterparts are vibrational, rotational and magnetic quantum numbers, θ is the scattering angle (the angle between **k** and **k′**, the reactant-approach and product-recoil directions), and E_{coll} is the collision energy. In detailed stereodynamical studies, however, it is convenient to

think about the chemical reaction as being described by the process

$$A + BC(v, j, k, q) \xrightarrow{E_{coll},\theta} AB(v', j', k', q') + C \qquad (2)$$

where k, q, and their primed counterparts are labels associated with the rotational polarization moments that characterize the relative directions of motion of reactants and products.[17−30] Because our interest here lies in reactant rather than product polarization, the values of the product-polarization labels are fixed at $k' = q' = 0$ (this means that products are considered regardless of their polarization state), and hereafter not explicitly mentioned. Note also that we have ignored electronic and nuclear spins, which means that the methods and results to be presented below will be valid only when the BC reactant is a closed-shell molecule not susceptible to fast hyperfine depolarization.[22−24,39−45]

There are four main reasons for the replacement of magnetic quantum numbers by polarization moments. Two are technical, and the other two are practical. The first technical reason is that the mathematical description of the dependence of reaction dynamics on spatial directions requires the extensive use of angular momentum algebra, which is made easier by the introduction of polarization moments.[23,27] Very loosely speaking, this has to do with the fact that polarization moments are always explicitly related to all three spatial directions comprising the *xyz* reference frame, whereas magnetic quantum numbers are explicitly related to only one spatial direction (the quantization axis, *z*). The second technical reason is that, because classical mechanics cannot deal with phases of angular momentum states, it is not possible to formulate a complete quasiclassical theory of reaction stereodynamics in terms of magnetic quantum numbers; if one wants to maximize the benefit from direct comparisons of quantum and quasiclassical results, the two theories must be stated in similar terms. The first practical reason is that polarization moments relate to the results from experiments regarding chemical stereodynamics more directly than populations and phases of magnetic states. The second practical reason is that, to some extent, polarization moments describe directional effects in more intuitive terms (orientation and alignment of molecular axes and rotational angular momenta[18,20,22,24,46,47]) than magnetic quantum numbers. This is the case at least for the first few orientation or alignment moments, which at present are the ones attracting more attention.

The theory we present here is based on what we call "extrinsic" and "intrinsic" polarization moments. Extrinsic polarization moments describe actual reactant preparation schemes and quantify the anisotropies of the rotational angular momentum and molecular axis distributions in the asymptotic region where reactants do not yet interact. Extrinsic polarization moments are a consequence of external circumstances (the experimental setup) rather than the reaction itself; they have nothing to do with the collision dynamics. We might as well call them "prepared" polarization moments.

In contrast, intrinsic polarization moments describe the reactive process itself. They quantify the dependence of the reaction cross section on the anisotropies of the rotational angular momentum and molecular axis distributions of the reactants. Intrinsic polarization moments are determined by the collision dynamics rather than by external circumstances (the experimental setup). We might as well call them "dynamical" polarization moments.

The distinction between intrinsic and extrinsic properties can be made clearer by consideration of a more familiar example: the scattering (S) matrix obtained in reactive scattering calculations. In the terms used in this article, the S matrix is an intrinsic quantity because it describes the connections (rigorously speaking, transition probability amplitudes) tying reactants to products rather than the reactants state considered in a particular study. The S matrix does not depend on whether one is interested in reactions involving rotationally excited reactants or not. Of course, the values of observable properties (say, integral cross sections) cannot be calculated unless the reactants state (the extrinsic property) is determined. But the dynamical information is in the intrinsic property (the scattering matrix), not in the extrinsic one (the reactants state).

Metaphorically speaking, one might say that intrinsic properties express what the reaction wants, whereas extrinsic properties express what the reaction gets. Reaction cross sections depend on both.

2.1. Reference Frames. Unless otherwise stated, all of the results below are referred to a center-of-mass *xyz* frame in which the *z* axis is parallel to the reactant-approach direction, **k**, *xz* is the scattering plane containing both **k** and the product-recoil direction, **k′**, and the *y* axis is parallel to **k** × **k′**. We shall refer to this *xyz* system of axes as the "scattering frame," and use a lowercase q to represent the polarization moment components defined with respect to the scattering frame and lowercase θ_j and φ_j to represent the polar and azimuthal angles that describe the direction of the reactant diatomic rotational angular momentum vector, **j**, in the scattering frame. Similarly, the direction of the reactant diatomic internuclear axis in this frame will be given by θ_r and φ_r.

When dealing with possible experimental situations, we will also need to consider an *XYZ* "laboratory frame," whose origin coincides with the scattering frame but whose spatial orientation is fixed; its explicit definition will be presented in Section 4. We shall use an uppercase Q to represent the polarization moment components defined with respect to the laboratory frame and uppercase Θ_j and Φ_j to represent the polar and azimuthal angles that describe the direction of the rotational angular momentum vector, **j**, in the laboratory frame.

We choose to represent the relationship between the two frames in terms of the rotation that takes *xyz* into *XYZ* (not the rotation that takes *XYZ* into *xyz*) and represent the Euler angles that define this rotation by α, β, and γ. It follows that β and α are the polar and azimuthal angles that describe the orientation of Z in the scattering frame.

2.2. Intrinsic Reactants PDDCS. The most important quantities for our reactant polarization analysis method are the intrinsic polarization moments we represent by $S_q^{(k)}(\theta)$ and $S_{q\pm}^{\{k\}}(\theta)$. They are, respectively, complex and real versions of the same thing, mutually related by

$$S_{q+}^{\{k\}}(\theta) = \frac{1}{\sqrt{2}}[(-1)^q S_q^{(k)}(\theta) + S_{-q}^{(k)}(\theta)] = (-1)^q\sqrt{2}\,\mathrm{Re}[S_q^{(k)}(\theta)], \qquad 1 \le q \le k \qquad (3a)$$

$$S_{q-}^{\{k\}}(\theta) = \frac{1}{i\sqrt{2}}[(-1)^q S_q^{(k)}(\theta) - S_{-q}^{(k)}(\theta)] = (-1)^q\sqrt{2}\,\mathrm{Im}[S_q^{(k)}(\theta)], \qquad 1 \le q \le k \qquad (3b)$$

$$S_0^{\{k\}}(\theta) = S_0^{(k)}(\theta) \qquad (3c)$$

These polarization moments quantify the dependence of the differential cross section (DCS) on the polarization of the

reactants. Maintaining a term already in use,[18] we call them the "intrinsic reactants PDDCSs," where the acronym stands for "polarization-dependent differential cross section".

Complex polarization moments are best for mathematical manipulations but are not directly associated with Cartesian directions[50] or observable differential cross sections (the corresponding operators are not Hermitian). Real polarization moments are cumbersome for mathematical manipulations but are directly associated with Cartesian directions and observable differential cross sections (the corresponding operators are Hermitian). We therefore use this approach: derivations and calculations are done with complex polarization moments, but numerical results and figures are presented in terms of real polarization moments.

As already mentioned, the labels k and q identify particular rotational polarization moments of the reactants. The rank k identifies the particular type of multipole under consideration: $k = 0$ for a monopole, $k = 1$ for a dipole, $k = 2$ for a quadrupole, and so on up to $k = 2j$. The component q identifies the spatial direction(s) associated with each multipole. Each intrinsic reactants PDDCS, $S_q^{(k)}(\theta)$, quantifies the dependence of the differential cross section on a particular type of reactants polarization; the details of the particular directions and types of polarization associated with each combination of k and q values when $k \leq 2$ can be found in ref 18.

For future reference, we also note that the complex polarization moments satisfy the following relation:

$$[S_q^{(k)}(\theta)]^* = (-1)^q S_{-q}^{(k)}(\theta) \tag{4}$$

If, in addition, the distribution of internuclear axis is invariant to reflection in the xz scattering plane, as in atom−diatom collisions, it holds that

$$S_q^{(k)}(\theta) = (-1)^{k+q} S_{-q}^{(k)}(\theta) = (-1)^k [S_q^{(k)}(\theta)]^* \tag{5}$$

which in combination with eq 3 implies that the only nonvanishing real polarization moments are

$$k \text{ even: } S_0^{(k)} \text{ and } S_{q+}^{\{k\}}, \qquad 1 \leq q \leq k \tag{6a}$$

$$k \text{ odd: } S_{q-}^{\{k\}}, \qquad 1 \leq q \leq k \tag{6b}$$

We close this Section by stressing that the intrinsic reaction PDDCS is an intrinsic property that gives information about the reaction dynamics. Its numerical value cannot be directly measured. To obtain numbers that can be measured (i.e., observable reaction properties), one must take into account an extrinsic property: the actual polarization of the reactants, which we will consider before showing how observable differential cross sections can be calculated.

2.3. Polarization of Reactants. When the directions of the angular momenta are prepared prior to the collision, one must consider the actual polarization of the reactants. This is an extrinsic property: instead of depending on the reaction dynamics, it depends on external intervention.

The polarization of the BC reactant in reaction 2 is described by a set of polarization moments that we denote by $a_q^{(k)}$ or $a_{q\pm}^{\{k\}}$ when using the complex or real representations. Because these polarization moments are to be used in conjunction with intrinsic properties such as the one discussed in the previous section, the two must be defined with respect to the same reference frame.

Suppose that (as is done in this paper) one wants to study the reaction dynamics in the xyz scattering frame and that all intrinsic properties are referred to xyz. If reactants are produced in the laboratory with complex polarization moments, $A_Q^{(k)}$, referred to the XYZ space-fixed frame, then a frame transformation is required: one must use the values of the laboratory polarization moments, $A_Q^{(k)}$, to determine the values of the scattering-frame polarization moments, $a_q^{(k)}$. The formula for this transformation is

$$a_q^{(k)} = \sum_{Q=-k}^{k} D_{qQ}^{k*}(\alpha, \beta, \gamma)\, A_Q^{(k)} \tag{7}$$

where $D^k(\alpha, \beta, \gamma)$ is a Wigner rotation matrix and α, β, and γ are the Euler angles associated with the rotations that take the xyz scattering frame into the XYZ laboratory frame (see Section 2.1). As is always the case in angular momentum algebra, one must be careful with the conventions and definitions used. Equation 7 is valid when (i) the rotation matrix follows the conventions of ref 50 and (ii) the complex polarization moments are defined as covariant components of the polarization tensor (this is the definition we use throughout this work, see Section 3).

Real polarization moments can be obtained from their complex counterparts by the use of expressions entirely analogous to those in eq 3.

2.4. Observable DCS. Once the intrinsic reactants PDDCSs and the (extrinsic) reactants polarization moments have been calculated, one must combine them in order to obtain the observable differential cross section. The formula required is

$$\frac{d\sigma}{d\omega} = \frac{\sigma_{iso}}{2\pi} \sum_{kq} (2k+1)[S_q^{(k)}(\theta)]^* a_q^{(k)} \tag{8}$$

where $d\sigma/d\omega$ is the DCS, and σ_{iso} the integral cross section of the reaction involving unpolarized reactants, in other words, the reaction in which the spatial distributions of the rotational angular momentum and internuclear axis of the BC reactant are isotropic.

2.5. Meaning of Intrinsic Reactants PDDCSs. To further clarify the information content of eq 8, let us consider the particular case of unpolarized reactants. In this case, the extrinsic reactant polarization moments are given by

$$\text{unpolarized reactants: } a_q^{(k)} = \delta_{k0}\delta_{q0} \tag{9}$$

and we have

$$\frac{d\sigma}{d\omega} = \frac{\sigma_{iso}}{2\pi} S_0^{(0)}(\theta) \tag{10}$$

That is, the intrinsic reactants PDDCS, $S_0^{(0)}(\theta)$, gives the product angular distribution of the reaction involving unpolarized reactants. In other words, $S_0^{(0)}(\theta)$ gives the probability of observing reaction when the angle between the reactant-approach and product-recoil directions is θ. Note that in order to obtain the integral cross section from eq 10, one must integrate it not only over $\cos\theta$ but also over the azimuthal angle, φ, hence the need for the 2π factor.

What about the other intrinsic PDDCSs? Equation 8 shows that each $S_q^{(k)}(\theta)$ quantifies the extent to which the corresponding extrinsic reactant polarization moment, $a_q^{(k)}$, leads to a distortion of the differential cross section. Another important

observation is that, when PDDCSs with $k > 0$ are included, probability is not conserved: in general

$$\int_{-1}^{1} S_q^{(k)}(\theta)\, \mathrm{d}(\cos\theta) \neq 0 \tag{11}$$

Extrinsic reactants polarization will, in general, lead not only to a different shape for the differential cross section (i.e., to a different product angular distribution) but also to a different reaction probability and to a different integral cross section. The intrinsic reactants PDDCSs quantify the reaction sensitivity to both effects. In short, they quantify the intrinsic stereochemistry of the reaction.

2.6. Renormalized PDDCSs. As just described, intrinsic reactants PDDCSs allow us to calculate how product angular distributions and reaction cross sections change with reactants polarization. They do not, however, express this in relative terms.

This point is better explained with an example. Suppose that we calculate the value of a given $S_q^{(k)}(\theta)$, say $S_0^{(2)}(\pi/2)$, and obtain 3.2. Does that mean that the alignment of the BC rotational angular momentum along the z direction has a dramatic effect on the reaction or only a minor one? As it turns out, the value of the intrinsic PDDCS does not provide a direct answer to this question. To answer it, we need renormalized PDDCSs

$$\text{renormalized PDDCS: } \frac{S_q^{(k)}(\theta)}{S_0^{(0)}(\theta)} \tag{12}$$

The importance of renormalized PDDCSs comes from the fact that they have well-defined ranges of allowed values.[18] The closer the calculated values are to the limits (positive or negative) of the allowed ranges, the more sensitive the reaction is to polarization effects. If renormalization of the PDDCS mentioned above leads to a small value (say, $S_0^{(2)}(\pi/2)/S_0^{(0)}(\pi/2) = 0.02$) we can say that the reaction is rather insensitive to this kind of reactant polarization. But if the renormalization leads to a large value (say we are doing a classical calculation and obtain $S_0^{(2)}(\pi/2)/S_0^{(0)}(\pi/2) = 0.97$, a value very close to 1, the upper classical limit for this k and q values[18]), then we can say that the reaction is very sensitive to this kind of reactant polarization. To give meaning to terms such as "large sensitivity," we need to ask ourselves: large relative to what? That is where the renormalized PDDCSs step in. The question they address is this: *relative to the reactivity associated with unpolarized reactants*, how large or small is the reactivity one can get by polarizing them?

2.7. Intrinsic Reactants PP. To quantify the effect of reactants polarization on the integral cross section, it is convenient to introduce the polarization moments that we represent by $s_q^{(k)}$ and, again, maintaining a term already in use, call the "intrinsic reactants PPs" (the acronym stands for "polarization parameter"). They are defined by

$$s_q^{(k)} = \int_{-1}^{1} S_q^{(k)}(\theta)\, \mathrm{d}(\cos\theta) \tag{13}$$

2.8. Observable ICSs. Once the intrinsic reactants PPs and the (extrinsic) reactants polarization moments have been calculated, one can combine them in order to obtain observable integral cross sections. Before doing that, however, one must note that the introduction of reactants polarization leads to two different possibilities regarding the definition of integral cross sections.

To understand this problem, one must start by realizing that the correlation between the **k** and **k′** vectors, as is always the case for two-vector correlations,[26] is a function of one angle only: in this case, the scattering angle, θ. This leads to the familiar result that DCSs of reactions involving unpolarized reactants are always independent of the azimuthal angle, φ, and that integration over this angle amounts to no more than multiplication by a factor of 2π.

A complication arises, however, when one wants to consider reactants polarization as well as the reactant-approach and product-recoil directions. This amounts to consideration of the **j**−**k**−**k′** three-vector correlation, which depends on three angles.[26] There are two natural ways to choose the set of angles:

A. As $\{\theta, \theta_j, \varphi_j\}$. (Here θ is the angle between **k** and **k′**, whereas θ_j is the angle between **k** and **j**, and φ_j is the dihedral angle specifying the location of the plane containing **k** and **j** with respect to the reference, scattering plane containing **k** and **k′**.)

B. As $\{\theta_j, \theta, \varphi\}$. ($\theta$ and θ_j as above; φ is the dihedral angle specifying the location of the scattering plane containing **k** and **k′** with respect to the reference plane containing **k** and **j**. Note that the reference plane is not the same as in case A.)

Although both choices are possible, and mathematically equivalent, practical issues introduce a clear bias in favor of scheme A, which is indeed the one we have used so far: our expression for the DCS, eq 8, is independent of φ.

The question is less easily addressed, however, when one wants to "reduce" the differential cross section describing the **j**−**k**−**k′** correlation to the integral cross section describing the **j**−**k** correlation. This must be done by integration over θ and φ. But what differential cross section must be integrated, the one obtained with scheme A or the one obtained with scheme B? The integration results are not equivalent.

The important point to note is that the DCS associated with scheme A, the one of eq 8, does not depend on φ. Integration over this angle amounts to a simple multiplication by 2π, and does not remove the azimuthal dependence on the dihedral angle, φ_j. However, the DCS associated with scheme B (its mathematical expression is not included in this paper) does depend on φ, which in this case is also the dihedral angle associated with azimuthal asymmetry. Integration over φ therefore does not amount to a simple multiplication by 2π, and completely removes the azimuthal dependence.

Our answer to the question of which integration should be performed is based again on practical issues, and is the following: both, because the resulting integral cross sections do not convey the same information and are both measurable.

Let us first deal with scheme A. Integration of eq 8 over cos θ and φ yields

$$\tilde{\sigma} = \sigma_{\mathrm{iso}} \sum_{kq} (2k+1)[s_q^{(k)}]^* a_q^{(k)} \tag{14}$$

a quantity we will refer to as the *special* ICS. The reason for the "special" qualifier is that the value of $\tilde{\sigma}$, contrary to the value of σ (the "ordinary" ICS to be discussed shortly), is not completely independent of the product-recoil direction, **k′**. This is because the determination of $\tilde{\sigma}$, although not requiring specification of the exact direction of **k′**, does require specification of the location of the scattering plane containing **k** and **k′** because the dihedral angle associated with azimuthal asymmetry is defined with respect to the scattering plane. Experimentally, the special ICS can only be measured indirectly, by integration of a (directly measurable) differential cross section. It cannot be determined when product detection does not discriminate

recoil direction. Another noteworthy point is that the special ICS does not express the "pure" $\mathbf{j}-\mathbf{k}$ two-vector correlation because determination of the value of $\tilde{\sigma}$ requires specification of two angles (θ_j and φ_j) rather than only one angle.

From the experimental point of view, the integral cross sections associated with scheme B are the more natural ones because they are truly independent of the product-recoil direction. They can be measured directly (by product detection irrespective of recoil direction) because knowledge of the position of the scattering plane is not necessary. The formula required for their calculation is

$$\sigma = \sigma_{\text{iso}} \sum_k (2k+1) s_0^{(k)} a_0^{(k)} \tag{15}$$

(the complex conjugate symbol has been dropped because the polarization moments with $q = 0$ are real). Note that the difference between σ and the special ICS of eq 14 is that polarization moments with $q \neq 0$ do not contribute to the value of σ; in other words, σ does not convey dihedral information. The reason is that the loss of information about the location of the scattering plane prevents one from creating azimuthally asymmetric reactant polarizations and the information about the $s_q^{(k)}$ with $q \neq 0$ is lost.

Note also that the above discussion uses arguments exclusively drawn from the intrinsic distribution of angular momentum. An alternative deduction can be made using the extrinsic point of view. From this perspective, the φ azimuthal angle defines the dihedral angle between the $\mathbf{kk}'$ (xz) scattering plane and, in principle, any arbitrary, "external" reference plane. In particular, it is possible to refer the scattering frame to the actual *XYZ* laboratory frame because the properties calculated on the former will depend on the relative orientation of both frames as long as an extrinsic polarization exists. The dihedral angle between the *xz* and *XZ* planes is α. Therefore, *with respect to the XYZ frame*, the φ angle will be $2\pi - \alpha$.

Considering the relationship between the laboratory polarization moments and those in the scattering frame given by eq 7 and substituting in eq 8, the expression of the DCS becomes a function of the Euler angles that relate the scattering and the laboratory frame. By integration of eq 8 over $\cos\theta$ and φ or α, only those moments with $q = 0$ survive. By using eq 7 again, eq 15 is recovered.

2.9. Meaning of Intrinsic Reactants PPs. By using a procedure analogous to the one in Section 2.5, we show that we must have

$$s_0^{(0)} = 1 \tag{16}$$

and that the remaining intrinsic reactant PPs quantify the sensitivity of the integral reaction cross sections to the extrinsic reactant polarization.

We also note that in this case we do not need to define "renormalized PPs" in order to obtain the kind of relative information discussed in Section 2.6. As suggested by eq 16, our definitions imply that the intrinsic reactants PPs are "naturally renormalized" and therefore convey relative as well as absolute information directly.

2.10. Stereodynamical Portraits. The PDDCSs and PPs we have just introduced are the parameters that quantify the reaction stereodynamics. Quantitative parameters, however, are not always the best-suited ones, and certainly not the only ones that matter, when what one is after is qualitative understanding.

The point we are trying to make can be explained with an analogy. It involves a true story, in which the main characters are the youngest of the authors of this paper (James Haigh) and the author of some of the most influential papers in the field of stereodynamics, Dudley Herschbach. James has never met Professor Herschbach. While going through the mandatory introductory stereodynamics literature, James was impressed by Professor Herschbach's seminal articles and also by the frequent praise of his work in articles by other people. James got curious, and asked co-workers what Professor Herschbach looks like. Now we ask our readers: what would have been the best way to answer? To present James with an exhaustive list of anthropometric data (height, weight, etc.) or to show him a portrait of Professor Herschbach? No prizes for guessing what we did. Granted, an exhaustive list of anthropometric data might have been more quantitative, but would not have been nearly as effective as the portrait.

The situation is not too different with regard to chemical reactions. Although PDDCSs and PPs are certainly the parameters one needs to consider for a quantitative description of the reaction stereodynamics, a "portrait" of it conveys the overall situation in a much more effective and direct manner. So the question we have to address is this: how can one directly portray the stereodynamics of a chemical reaction? The answer is, by plotting the reaction's intrinsic spatial distributions of internuclear axes and rotational angular momenta.

If the intrinsic polarization moments are known, then so are the intrinsic spatial distributions of the rotational angular momentum vectors and internuclear axes. Now, *these are distributions that explicitly describe and graphically represent the dependence of the reaction dynamics on directions in space.* In our (admittedly fanciful) terms, these distributions are portraits of the reaction stereodynamics, of which some examples will be presented in Section 5.1.

Let us first consider internuclear axis ($\mathbf{r}$) distributions. They are related to the polarization moments by[51]

$$P(\theta_r, \varphi_r) = \sum_{k=0}^{2j} \sum_{q=-k}^{k} \frac{2k+1}{4\pi} s_q^{(k)} \langle j0, k0|j0\rangle C_{kq}^*(\theta_r, \varphi_r) \tag{17}$$

where $P(\theta_r, \varphi_r)$ is the probability density function (PDF) that directly describes the spatial distribution of the internuclear axis, θ_r and φ_r are the spherical angles that specify the direction of vector $\mathbf{r}$ in the chosen reference frame, $\langle j0, k0|j0\rangle$ are Clebsch−Gordan coefficients, and $C_{kq}^*(\theta_r, \varphi_r)$ are complex conjugates of modified spherical harmonics. Note that in this formula we have used the intrinsic reactants PPs as the polarization moments, but we might as well have used the PDDCSs, whether renormalized or not.

Rotational angular momentum ($\mathbf{j}$) distributions, in turn, are related to polarization moments by[46,47]

$$Q(\theta_j, \varphi_j) = \sum_{k=0}^{2j} \sum_{q=-k}^{k} \frac{2k+1}{4\pi} s_q^{(k)} \langle jj, k0|jj\rangle C_{kq}^*(\theta_j, \varphi_j) \tag{18}$$

where the $Q(\theta_j, \varphi_j)$ notation indicates that the PDF we are dealing with here is a *population distribution* rather than a probability density function (see refs 46 and 47 for a discussion of the need for this distinction). Again, we have used the intrinsic reactants PPs as the polarization moments, but we might as well have used PDDCSs, renormalized or not.

3. Calculation of PDDCS

In the previous section, we showed that the central quantities in our theory are the intrinsic reactants PDDCSs. We have also

shown how other important quantities (renormalized PDDCSs, polarization parameters, cross sections, and stereodynamical portraits) can be obtained once the PDDCSs are known. What we have not yet described is how the $S_q^{(k)}(\theta)$ values can actually be calculated, and this is what this section is devoted to.

The intrinsic reactants PDDCSs can be calculated with both quantum and quasiclassical methods. Quantum calculations (we assume them to be time-independent calculations or else time-dependent calculations capable of producing scattering matrixes as their output[53−56]) describe the reaction dynamics intrinsically; the result of the calculation is a scattering matrix. This means that intrinsic reaction properties can be obtained directly, without recourse to extrinsic properties (which in this case would be the density matrices defining actual states of reactants and products).

As for quasiclassical trajectory (QCT) calculations, they are carried out using a uniform distribution of the rotational angular momentum or internuclear axis, without any polarization bias. Of course, each individual trajectory is associated with given initial and final polarization states, but the ensemble of trajectories spans a uniform, isotropic distribution of directions. It is the analysis of the subset of trajectories tying given initial and final rovibrational states of reactants and products that provides the information with respect to the intrinsic propensity of a given initial distribution of angular momenta to produce a particular final state.

In this section, we describe the calculations as we actually did them and do not emphasize the similarities between the quantum and quasiclassical descriptions; readers interested in a presentation highlighting these similarities are referred to one of our earlier papers, ref 18.

We also note that we are now about to enter a part of the article that, although important for a rigorous justification of our theory and also for actual calculations, is not essential for an understanding of the kind of information one can obtain by using it. Readers interested in the former are invited to read on, but those with less demanding interests may wish to move on to Section 4.

3.1. Classical Mechanics. The classical description of the problem we are considering here (the three-vector $\mathbf{j}-\mathbf{k}-\mathbf{k}'$ correlation) starts with the definition of the classical probability density function $P_r(\theta, \theta_j, \varphi_j)$. This PDF (an intrinsic reaction property) gives the probability of observing reactive scattering from given reactants rovibrational states into given products rovibrational states and at scattering angle θ when the initial direction of the BC reactant rotational angular momentum is the one associated with spherical angles θ_j and φ_j. The classical reaction PDF is dimensionless, normalized to unity

$$\int_{-1}^{1}\int_{0}^{2\pi}\int_{-1}^{1} P_r(\theta, \theta_j, \varphi_j)\, \mathrm{d}(\cos\theta_j)\, \mathrm{d}\varphi_j\, \mathrm{d}(\cos\theta) = 1 \quad (19)$$

and as such can be expanded as a series of spherical harmonics[50,52] in the form

$$P_r(\theta, \theta_j, \varphi_j) = \sum_{k=0}^{\infty}\sum_{q=-k}^{k} \frac{2k+1}{4\pi} S_q^{(k)}(\theta)\, C_{kq}^*(\theta_j, \varphi_j) \quad (20)$$

where the θ-dependent expansion coefficients are the intrinsic reactants PDDCSs introduced in Section 2.2.

By using the orthogonality of the spherical harmonics to invert eq 20, one gets the following expression:

$$S_q^{(k)}(\theta) = \int_0^{2\pi}\int_{-1}^{1} P_r(\theta, \theta_j, \varphi_j)\, C_{kq}(\theta_j,\phi_j)\, \mathrm{d}(\cos\theta_j)\, \mathrm{d}\varphi_j \quad (21)$$

The reaction differential cross section (which must take into account an actual, extrinsic reactant preparation scheme as well as the intrinsic reactants PDDCS) is given by

$$\frac{\mathrm{d}\sigma}{\mathrm{d}\omega} = \frac{\sigma_{\mathrm{iso}}}{2\pi}\int_0^{2\pi}\int_{-1}^{1} 4\pi P(\theta,\theta_j, \varphi_j)\, \rho(\theta_j, \varphi_j)\, \mathrm{d}(\cos\theta_j)\, \mathrm{d}\varphi_j \quad (22)$$

where σ_{iso} is the integral cross section of the reaction involving unpolarized reactants (which must be divided by 2π in order to take into account the fact that the differential cross section is independent of φ), $\rho(\theta_j, \varphi_j)$ is the PDF describing the extrinsic reactants polarization, and the 4π factor inside the integral ensures its correct normalization.

The extrinsic reactants PDF can be expanded in a multipolar series entirely similar to the one used for the intrinsic one, eq 20

$$\rho(\theta_j, \varphi_j) = \sum_{k=0}^{\infty}\sum_{q=-k}^{k} \frac{2k+1}{4\pi} a_q^{(k)}\, C_{kq}^*(\theta_j, \varphi_j) \quad (23)$$

where the $a_q^{(k)}$ values are the extrinsic reactant polarization moments introduced in Section 2.3. Inserting eqs 20 and 23 in eq 22, one obtains

$$\frac{\mathrm{d}\sigma}{\mathrm{d}\omega} = \frac{\sigma_{\mathrm{iso}}}{2\pi}\sum_{k'k}\sum_{q'q} \frac{(2k+1)(2k'+1)}{4\pi} S_q^{(k)*}(\theta)\, a_{q'}^{(k')} I \quad (24)$$

where

$$I = \int_0^{2\pi}\int_{-1}^{1} C_{kq}(\theta_j, \varphi_j)\, C_{k'q'}^*(\theta_j, \varphi_j)\, \mathrm{d}(\cos\theta_j)\, \mathrm{d}\varphi_j = \frac{4\pi}{2k+1}\delta_{k'k}\delta_{q'q} \quad (25)$$

Inserting this last equation in eq 24 finally gives us eq 8, the expression for observable differential cross sections in terms of the intrinsic reactants PDDCSs and the extrinsic reactants polarization moments.

Now that the formal definitions have been presented, we turn to actual numerical calculations. The procedure can be summarized as follows. Each particular combination of reactant and product rovibrational states is considered in turn, along with the corresponding subset of trajectories. This subset contains $N_{vjv'j'}$ trajectories, labeled by the index i. The values of the scattering angle $\theta^{(i)}$ and the polar and azimuthal angles that define the direction of $\mathbf{j}$, $\theta_j^{(i)}$, and $\phi_j^{(i)}$, are determined for each of the $N_{vjv'j'}$ trajectories. This information is used to calculate the values of all of the modified spherical harmonics of interest for each trajectory, and then the trajectory-specific values are averaged over the $N_{vjv'j'}$ reactive trajectories.

In practice, this is done by expressing the PDDCSs as a series of modified spherical harmonics[18,52]

$$S_q^{(k)}(\theta) = \frac{1}{2}\sum_{k_1\geq|q|} (2k_1+1)\, s_{kq}^{k_1}\, C_{k_1-q}(\theta, 0) \quad (26)$$

where the $s_{kq}^{k_1}$ coefficients are given by

$$s_{kq}^{k_1} = \langle C_{k_1-q}(\theta, 0)\, C_{kq}(\theta_j, \varphi_j)\rangle$$

$$\approx \frac{1}{N_{vjv'j'}} \sum_{i=1}^{N_{vjv'j'}} C_{k_1-q}(\theta^{(i)}, 0)\, C_{kq}(\theta_j^{(i)}, \varphi_j^{(i)}) \qquad (27)$$

The PPs are evaluated as[18]

$$s_q^{(k)} = \langle C_{kq}(\theta_j, \varphi_j)\rangle = \frac{1}{N_{vjv'j'}} \sum_{i=1}^{N_{vjv'j'}} C_{kq}(\theta_j^{(i)}, \varphi_j^{(i)}) \qquad (28)$$

As above, the brackets indicate the averaging over the whole set of trajectories associated with the chosen rovibrational states of reactants and products.

One more remark is needed before we conclude our presentation of the quasiclassical theory. Attentive readers may have noticed that the PDFs used in eqs 20 and 23 do not have the same form as the ones used for the generation of the stereodynamical portraits showing the intrinsic spatial angular momentum distribution (eq 18). The former are infinite series involving no Clebsch−Gordan coefficients; the latter is a finite series involving Clebsch−Gordan coefficients. The reason is this: eqs 20 and 23 are purely classical expressions used in a classical calculation. Equation 18 is a quantum-mechanical expression, used to turn the classical results into quasiclassical ones by forcing onto them a quantum mechanical restriction (in this case, a restriction of the extent to which the exact direction of an angular momentum vector can be specified, see refs 46 and 47). In a sense, this is analogous to the "boxing" procedure used to associate specific quantum numbers to molecules whose energy levels are not quantized in a classical calculation.

3.2. Quantum Mechanics. The starting point of our derivation of the quantum mechanical expression for the reactants intrinsic PDDCSs is a scattering matrix in the helicity representation, the one most naturally adapted for the description of the $\mathbf{j}-\mathbf{k}-\mathbf{k}'$ vector correlation.[17] Complete specification of a particular element of this matrix requires a notation such as $S^{EJM}_{a'v'j'\Omega',avj\Omega}$, with the various indices indicating the total energy (E), total angular momentum (J), projection (M) of $\mathbf{J}$ on a space-fixed axis, Z, and the arrangement, vibrational, rotational and helicity quantum numbers for the reactants (a, v, j, and Ω) and products (a', v', j', and Ω'). Because the S matrix elements are independent of M and the formulas used in this article only require implicit use of the energy, arrangement, and vibrational labels, we simplify the notation to $S^J_{j'\Omega',j\Omega}$.

Using this simplified notation, we can write the scattering amplitude as[57]

$$f_{\Omega'\Omega}(\theta) = \frac{1}{2ik_{\text{in}}} \sum_J (2J+1)\, \mathrm{d}^J_{\Omega'\Omega}(\theta)\, S^J_{j'\Omega',j\Omega} \qquad (29)$$

where $\mathrm{d}^J_{\Omega'\Omega}(\theta)$ is a reduced rotation matrix and k_{in} the wavenumber associated with the incoming (reactants) plane wave.

The differential cross section, allowing for an arbitrary reactants polarization (and therefore arbitrary coherence between the possible reactant helicities), is related to the scattering amplitude by[17]

$$\frac{\mathrm{d}\sigma}{\mathrm{d}\omega} = \sum_{\Omega'\Omega_1\Omega_2} f_{\Omega'\Omega_1}(\theta)\, f^*_{\Omega'\Omega_2}(\theta) \langle j\Omega_1|\rho|\, j\Omega_2\rangle \qquad (30)$$

where $\langle j\Omega_1|\rho|j\Omega_2\rangle$ is an element of the rotational-space density matrix of the reactants.

Readers should note three points about this formula, namely, (i) that we are disregarding product polarization and summing the DCS over product helicities, (ii) that we are assuming the reactants to be in a well-defined rotational energy level so that the only coherences playing any polarization role are those among different helicity substates, and (iii) that the DCS formula mixes intrinsic properties (scattering amplitudes) and extrinsic ones (reactants density matrix).

Using the expansion of the reactants density matrix that is the quantum analogue[18,46,47] of the classical expansion of eq 23, we get

$$\langle j\Omega_1|\rho|\, j\Omega_2\rangle = \sum_{k=0}^{2j} \sum_{q=-k}^{k} \frac{2k+1}{2j+1} a_q^{(k)} \langle j\Omega_1, kq|\, j\Omega_2\rangle \qquad (31)$$

Introducing this expression in eq 30, one obtains

$$\frac{\mathrm{d}\sigma}{\mathrm{d}\omega} = \sum_{k=0}^{2j} \sum_{q=-k}^{k} (2k+1)[U_q^{(k)}(\theta)]^* a_q^{(k)} \qquad (32)$$

where

$$[U_q^{(k)}(\theta)]^* = \sum_{\Omega'\Omega_1\Omega_2} f_{\Omega'\Omega_1}(\theta)\, f^*_{\Omega'\Omega_2}(\theta) \frac{\langle j\Omega_1, kq|\, j\Omega_2\rangle}{2j+1} \qquad (33)$$

Equation 32, although rather similar to the desired expression for the DCS (eq 8), is not quite there yet; the quantities represented here by $U_q^{(k)}(\theta)$ are not the dimensionless $S_q^{(k)}(\theta)$ values appearing in eq 8. To obtain that expression, we must multiply the right-hand side of eq 32 by

$$\frac{\sigma_{\text{iso}}}{2\pi} \frac{2\pi}{\sigma_{\text{iso}}} = 1 \qquad (34)$$

where σ_{iso}, the integral cross section of the reaction for an isotropic distribution of rotational angular momentum of the reactants summed over product helicities, is given by

$$\sigma_{\text{iso}} = \frac{\pi}{(2j+1)k_{\text{in}}^2} \sum_{J\Omega'\Omega} (2J+1)|S^J_{j'\Omega',j\Omega}|^2 \qquad (35)$$

as the reader can check by integrating eq 30 over $\cos\theta$ and φ while using

$$\langle j\Omega_1|\rho|\, j\Omega_2\rangle = \frac{\delta_{\Omega_1\Omega_2}}{2j+1} \qquad (36)$$

This finally gets us to eq 8, which in the quantum case must be used in conjunction with the following expression for the intrinsic reactants PDDCSs

$$[S_q^{(k)}(\theta)]^* = \sum_{\Omega'\Omega_1\Omega_2} \bar{f}_{\Omega'\Omega_1}(\theta)\, \bar{f}^*_{\Omega'\Omega_2}(\theta) \langle j\Omega_1, kq|j\Omega_2\rangle \qquad (37)$$

where the "scaled" scattering amplitudes are given by

$$\bar{f}_{\Omega'\Omega}(\theta) = \frac{\sum_J (2J+1)\, \mathrm{d}^J_{\Omega'\Omega}(\theta)\, S^J_{j'\Omega',j\Omega}}{[2\sum_{J\Omega'\Omega} (2J+1)|S^{\mathrm{J}}_{j'\Omega',j\Omega}|^2]^{1/2}} \qquad (38)$$

The formulas above, besides completing the derivation of the results necessary for the use of our theory in its quantum-

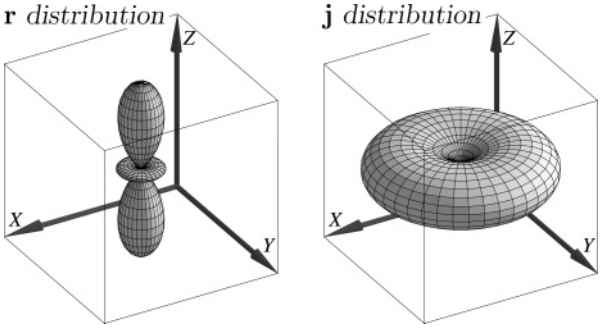

Figure 1. Spatial distributions of the interatomic axis, **r**, and the rotational angular momentum, **j**, of a diatomic molecule in a $|j = 2, m = 0\rangle$ state referred to the laboratory frame, *XYZ*.

mechanical version, justify our choice of notation for the intrinsic reactants PDDCSs. These are obtained by nothing more than a transformation of the scattering matrix, and one might argue that they are no more than visualizable versions of the *S* matrix that make the stereodynamical information explicit. We would agree with that remark, and that is why we chose to represent them by $S_q^{(k)}(\theta)$.

4. A Possible Experiment

This section describes what we believe to be a challenging yet feasible crossed-beam experiment that could be used to test our theoretical predictions and more specifically those regarding the role of D_2 alignment in the dynamics of the $H + D_2(v = 0, j = 2)$ reaction.

In Section 5, we will show that theory predicts D_2 alignment to have a dramatic effect on the collision outcome and that this effect will be clearly visible in differential cross sections, integral cross sections, and product state distributions. Because the experiment we propose can lead to the measurement of all of these quantities, if successfully carried out it will be capable of unambiguously demonstrating (or refuting) the rather striking theoretical predictions.

In simple terms, the experiment consists of the following: to place the molecules in the D_2 beam in the $|v = 0, j = 2, m = 0\rangle$ state, where the magnetic quantum number is determined with regard to a laboratory-fixed quantization axis, *Z*, whose direction can be chosen. This amounts to preparing $D_2(v = 0, j = 2)$ molecules whose interatomic axis is aligned parallel/antiparallel to *Z* and whose rotational angular momentum is aligned perpendicular to *Z*, see Figure 1. (This corresponds to positive axial alignment and negative rotational alignment. Note also that the **j** distribution depicted in Figure 1 is *exact*, not obtained with recourse to the vector model or some other approximation; see refs 46 and 47 for an explanation.) By varying the direction of the laboratory axis, *Z*, one varies its direction with regard to the scattering-frame vector, **k**, and, if the experiment involves angle-resolved product detection, also with regard to **k′** and therefore with regard to the scattering plane (the plane containing **k** and **k′**). Given that the laboratory axis, *Z*, is also the axis with regard to which the D_2 molecules are aligned, changing the direction of *Z* with regard to **k** and possibly **k′** amounts to changing the D_2 alignment in the scattering frame, and this is the basic idea of the experiment. Some of the technicalities are discussed further below, but first we will briefly reconsider the problem of how to express the laboratory **r** and **j** distributions in the scattering frame.

The first thing to consider is that the axial and rotational D_2 polarizations are both completely described by the molecular

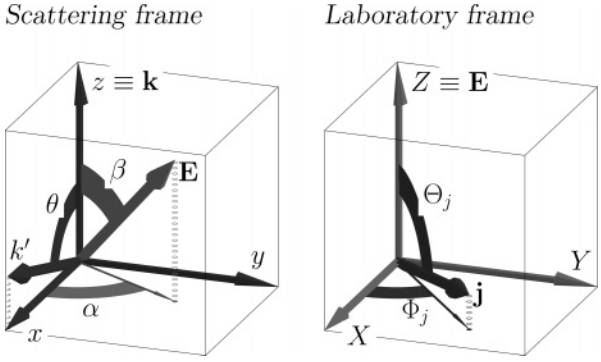

Figure 2. Scattering (*xyz*) and laboratory (*XYZ*) frames.

polarization moments, which when referred to the *XYZ* laboratory frame we represent by $A_Q^{(k)}$ (see Section 2.1). In the case considered here, the only nonvanishing moments are those with $k = 0$, 2, or 4 and $Q = 0$, and they take the values

$$A_0^{(0)} = 1, \quad A_0^{(2)} = -\sqrt{\frac{2}{7}}, \quad A_0^{(4)} = +\sqrt{\frac{2}{7}} \tag{39}$$

(As appropriate for an experiment, the values above are quantum-mechanical. The corresponding classical values are $A_0^{(0)} = 1$, $A_0^{(2)} = -1/2$, and $A_0^{(4)} = 3/8$.)

To obtain the extrinsic reactants polarization moments in the *xyz* scattering frame, all one has to do is to use eq 7. It leads to

$$a_q^{(k)} = D_{q0}^{k*}(\alpha, \beta, \gamma)\, A_0^{(k)} = C_{kq}(\beta, \alpha)\, A_0^{(k)} \tag{40}$$

Note that because the distributions we are considering have cylindrical symmetry around *Z* and therefore all nonvanishing $A_Q^{(k)}$ moments have $Q = 0$, the Euler angle γ does not play any role in the transformation and can be arbitrarily chosen. The only Euler angles required are α and β, the azimuthal and polar angles that specify the direction of the laboratory axis, *Z*, in the scattering frame. Figure 2, in which for reasons that will soon become clear, we have identified the direction of the laboratory axis, *Z*, as the direction of the electric field vector, **E**, presents a graphical illustration of how the Euler angles are defined and how the angles specifying the direction of the alignment axis and the angular momentum vector are defined in the scattering and laboratory frames.

The preparation of the $|j = 2, m = 0\rangle$ state can be achieved by pure rotational Raman scattering by selecting the right pump and Stokes laser frequencies for stimulated Raman scattering in a cell of D_2. By excitation via the $S(0)$ transition from $D_2(v = 0, j = 0)$, a considerable population of $D_2(v = 0, j = 2, m = 0)$ can be produced quite effectively by setting the polarizations of the stimulated Raman pump and Stokes lasers parallel to each other. The $S(0)$ transition results in the largest D_2 alignment that does not depend on the line strengths. The procedure proposed here is very similar to that used by Kandel et al.[19] in their study of the $Cl + HD(v = 1, j = 2)$ reaction. Sitz and Farrow have used a similar procedure to produce aligned N_2 in the $v = 1$ state.[65]

Associated with the $j = 2$ rotational state of D_2 are nuclear states with total spin $T = 0$ or $T = 2$, which can in principle lead to very strong hyperfine depolarization.[22−24,39−45] This effect, however, is not expected to be significant under the experimental conditions considered here. The reason is that collisions will occur within nanoseconds of reactant preparation but hyperfine depolarization will only occur in a microseconds time scale. Justification of this claim requires

consideration of the largest separation between $D_2(j = 2)$ hyperfine energy levels (185 kHz, see ref 66) and of the fact that the time scale for hyperfine depolarization[22,41,40] can be no shorter than the reciprocal of that value, that is, no shorter than 5 μs. This result is, of course, confirmed by detailed calculations.[43]

To minimize the presence of unpolarized $D_2(v = 0, j = 2)$ in the beam, one can expand pure *o*-D_2 through a nozzle cooled to liquid nitrogen temperature. This is known to produce more than 95% of D_2 molecules in the $v = 0, j = 0$ state. Although, at best, only 50% of the D_2 molecules can be excited into $|j = 2, m = 0\rangle$, the data acquisition can be done on a shot-to-shot basis with the excitation laser on/off or varying the polarizations of the pump and Stokes lasers to be either perpendicular or parallel.

Ideally, the experiment will be carried out in a high-resolution crossed molecular beam apparatus, similar to those used by Welge and co-workers[67] and by Yang and co-workers,[68] with a well-defined scattering plane. By varying the direction of the polarization vector, **E**, with respect to the relative velocity vector in β and the scattering plane in α, one can achieve different reactant polarizations in the *xyz* frame. Results from time-of-flight detection of the products at different laboratory scattering angles can be transformed into the center-of-mass system to obtain state-resolved differential cross sections and angle-recoil velocity polar maps. Moreover, by integrating the triple DCS (polar maps) in scattering angle and velocity, the special integral cross section could be determined for each geometry with different β and α angles.

We conclude this section by noting that the formulas necessary for the theoretical calculation of the cross sections that can be measured in this experiment are

$$\frac{d\sigma_{\alpha}^{\beta}}{d\omega} = \frac{\sigma_{iso}}{2\pi}\sum_{kq}(2k+1)[S_q^{(k)}]^* C_{kq}(\beta, \alpha) A_0^{(k)} \qquad (41)$$

$$\tilde{\sigma}_{\alpha}^{\beta} = \sigma_{iso}\sum_{kq}(2k+1)[s_q^{(k)}]^* C_{kq}(\beta, \alpha) A_0^{(k)} \qquad (42)$$

$$\sigma^{\beta} = \sigma_{iso}\sum_{k}(2k+1)s_0^{(k)} C_{k0}(\beta, 0) A_0^{(k)} \qquad (43)$$

These formulas are obtained by the insertion of eq 40 in eqs 8, 14, and 15, respectively. Note that, contrary to the $\tilde{\sigma}_{\alpha}^{\beta}$ special ICS, the σ^{β} ICS is independent of α. The mathematical reason for this is that the value of $C_{k0}(\beta, \alpha)$ is independent of α; the physical reason has been discussed in Section 2.8. Note also that, because this experiment involves D_2 alignment but not orientation (the only nonvanishing extrinsic polarization moments are those with *k* even, see eq 39), one can restrict the β and α ranges to

$$0° \le \beta \le 180° \qquad (44a)$$

$$0° \le \alpha \le 180° \qquad (44b)$$

and that the β range can be further reduced to

$$0° \le \beta \le 90° \qquad (45)$$

when the α-dependence is averaged out.

5. Illustrative Examples

There are three ways in which one can use the theory described in the previous sections. For reasons explained below, we call them the "intrinsic," "practical," and "min-max" approaches. Each of them has its own particular advantages, and it is likely that stereodynamical analyses will be easiest when all three are combined.

To illustrate the potential of each of those approaches, we have obtained numerical results, both quantum and quasiclassical, for the benchmark $H + D_2$ reaction. More specifically, we have considered the

$$H + D_2(v = 0, j = 2) \rightarrow HD(v', j') + D \qquad (46)$$

process at collision energies up to $E_{coll} = 1.7$ eV. The dynamical calculations, time-independent quantum reactive scattering and quasiclassical trajectories, both run on the BKMP2 potential energy surface,[58] have been described in earlier articles, and for this reason we do not repeat the descriptions here. Readers interested in the details of the quantum or quasiclassical calculations are advised to consult ref 59 for the former and refs 18 and 60 for the latter.

Besides choosing a particular reaction, we have selected our examples so that they highlight what can be achieved with the possible experiment we have described in Section 4.

We must stress, however, that the main purpose of this presentation is not to allow for a detailed analysis of the experiment or even of the role of D_2 polarization in reaction 46. Instead, our main purpose here is to provide illustrative examples of the kind of chemical information one can obtain by using the reactants polarization theory we have described.

5.1. The Intrinsic Approach: Insight and Understanding. When one wants to focus on the reaction stereodynamics itself rather than on a particular reactive process, the most natural way to approach the problem is to use the intrinsic approach described here. In the terms of the metaphor we have used in the beginning of Section 2, in the intrinsic approach one examines what the reaction wants rather than what it gets.

In the intrinsic approach, the extrinsic factor (the actual polarization of reactants) is ignored altogether. The questions one asks are these: what is the sensitivity of the reaction to reactants polarization? What polarizations are preferred? How anisotropic is the reaction dynamics? What is the *correlation* between the reactants polarization and reactivity?

The main advantage of the intrinsic approach is that it leads to clear pictures of the reaction mechanism itself, some of them of a rather intuitive nature. These are the "stereodynamical portraits" described in Section 2.10.

How does it work? The key idea has already been discussed (Sections 2.5 and 2.9): the intrinsic reactants PDDCSs and PPs quantify what the reaction wants. In less anthropomorphic terms, they quantify the correlation between the reactants polarization and the differential and integral reaction cross sections. Put in yet another way, the intrinsic reactants PDDCSs and PPs are the polarization moments of the reaction itself, rather than the polarization moments of actually existing reactants. And if we know these intrinsic polarization moments, then we can use them to plot the corresponding internuclear axis and rotational angular momentum distributions.

Figures 3 and 4 show some of these portraits, obtained with quantum polarization moments. In each of them, the left column shows "molecular axis portraits" (plots of the intrinsic dependence of the reaction on the direction of the internuclear axis of the D_2 reactant), whereas the right column shows "rotational portraits" (plots of the intrinsic dependence of the reaction on the direction of the rotational angular momentum of the D_2 reactant). Figure 3 shows the

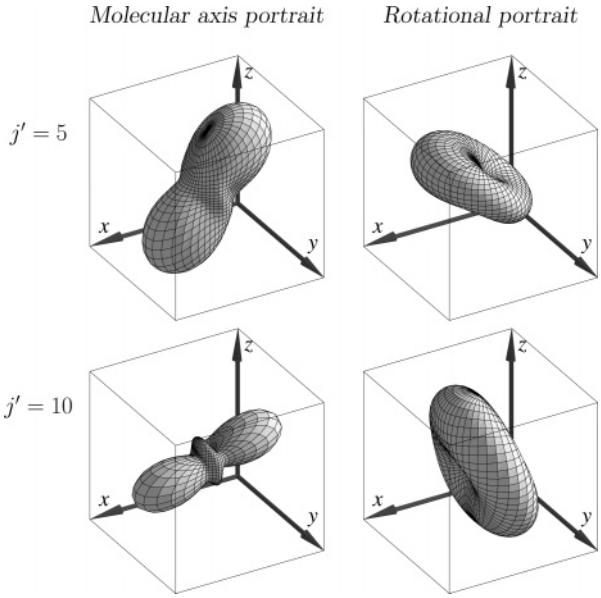

Figure 3. Stereodynamical portraits revealing the chemical shape of reaction 47 at $E_{coll} = 1.306$ eV with $j' = 5$ (top) or $j' = 10$ (bottom). The molecular axis portraits in the left column show the preferred distributions for the interatomic axis of the D_2 reactant, whereas the rotational portraits in the right column show the preferred distributions for the molecular rotational angular momentum. For the sake of clarity, the axes have been displaced from the center of each of the figures. See Section 2.1 for the definition of the *xyz* scattering frame.

results integrated over the scattering angle for the

$$H + D_2(v = 0, j = 2) \rightarrow HD(v' = 0, j') + D \qquad (47)$$

reaction with $j' = 5$ or $j' = 10$ and at $E_{coll} = 1.306$ eV, whereas Figure 4 shows θ-dependent results for the

$$H + D_2(v = 0, j = 2) \xrightarrow{\theta} HD(v' = 0, j' = 0) + D \qquad (48)$$

reaction obtained with $\theta = 4$, 8, or 11° and at the same collision energy. In other words, Figure 3 shows the $P(\theta_r, \varphi_r)$ and $Q(\theta_j, \varphi_j)$ functions obtained through use of the intrinsic PPs as the polarization moments in eqs 17 and 18, whereas Figure 4 shows the $P(\theta, \theta_r, \varphi_r)$ and $Q(\theta, \theta_j, \varphi_j)$ functions obtained through use of the intrinsic renormalized PDDCSs as the polarization moments in eqs 17 and 18.

In our opinion, pictures such as those in Figures 3 and 4 give the best possible representations of what back in 1990 Levine[61] called the "chemical shape" (as opposed to "physical shape") of a chemical reaction and as such fulfill one of the long standing dreams of chemical reaction stereodynamics: to determine the "shapes" of atoms and molecules *as perceived by each other* when they take part in a reactive collision.

Figures 3 and 4 also justify our use of the words "insight" and "understanding" in the heading of this section. A brief consideration of each of them does give significant insight into the reaction stereochemistry and also facilitates understanding of its mechanism. For instance, Figure 3 leads very naturally to the hypothesis that the amount of rotational energy of the HD product in reaction 47 is related to the collision geometry, with head-on reactive collisions leading to little product rotational excitation (cf. the $j' = 5$, top row of Figure 3) and side-on reactive collisions leading to larger product rotational excitation (cf. the $j' = 10$, bottom row of Figure 3). One might then speculate that this effect has to do with the amount of bending energy of the collision complex in the transition state region, although of course a thorough justification of such a claim would require a more detailed analysis, which is not the purpose of this article.

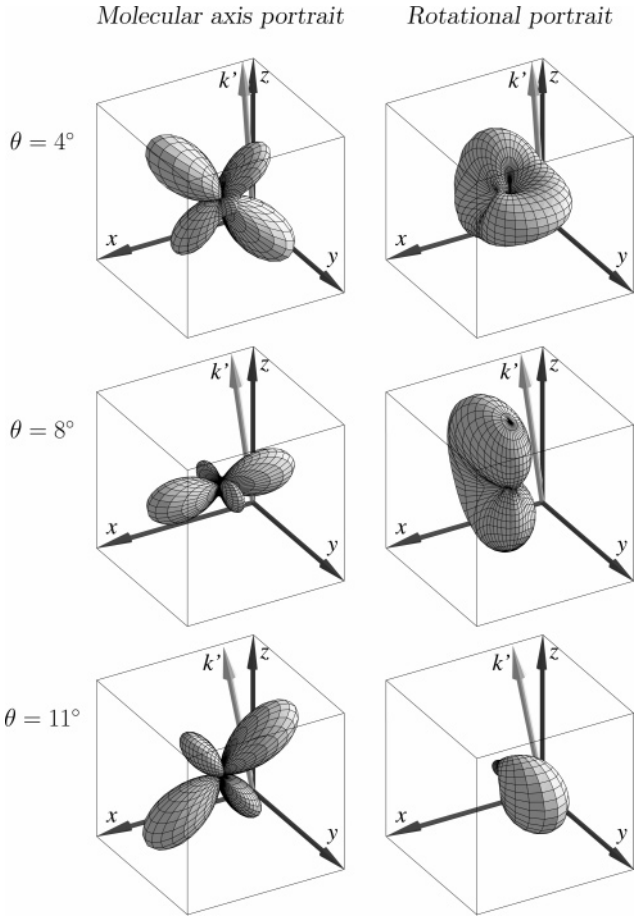

Figure 4. Stereodynamical portraits revealing the chemical shape of reaction 48 at $E_{coll} = 1.306$ eV and with $\theta = 4°$ (top), $\theta = 8°$ (middle), or $\theta = 11°$ (bottom). The molecular axis portraits in the left column show the preferred distributions for the interatomic axis of the D_2 reactant, whereas the rotational portraits in the right column show the preferred distributions for the molecular rotational angular momentum. The scattering angle, θ, between the reactant-approach and product-recoil directions is the angle between the vectors $\mathbf{k} \equiv z$ and $\mathbf{k}'$. As in Figure 3, the axes have been displaced from the center of each of the figures. See Section 2.1 for the definition of the *xyz* scattering frame.

Useful as they are in terms of qualitative understanding, the stereodynamical portraits presented above are not suitable for quantitative analyses. In quantitative terms, the key ingredients of the intrinsic approach to reaction stereodynamics are the intrinsic polarization-dependent differential cross sections (PDDCSs) and polarization parameters (PPs) introduced in Sections 2.2 and 2.7, which are the numerical parameters behind the stereodynamical portraits presented above.

Figures 5−7 show the PPs and renormalized PDDCSs calculated again at the $E_{coll} = 1.306$ eV collision energy. Each of these pictures includes both quantum and quasiclassical data, which allows for a quantitative assessment of the level of agreement between the two calculations.

Figures 5 and 6 show the real PPs of rank $k = 1$, 2, or 4, obtained for reaction 47 as a function of the HD product rotational state. As can be seen, the agreement between the quantum and quasiclassical PPs is impressive. Furthermore, these Figures show that the $s_0^{\{2\}}$ polarization parameter is the most relevant one for the differences found between the

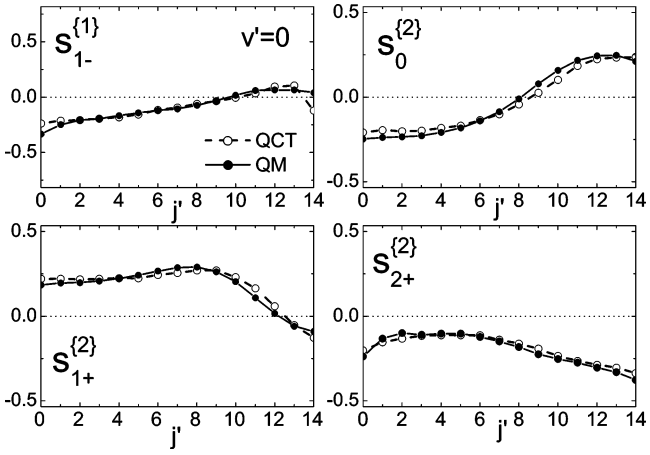

Figure 5. QM (solid line, solid circles) and QCT (dashed line, open circles) intrinsic polarization parameters of reaction 47 with $k = 1$, 2 at $E_{coll} = 1.306$ eV as a function of the HD product rotational state. The ranges of the vertical axes coincide with the allowed quantum ranges of these parameters for $j = 2$.

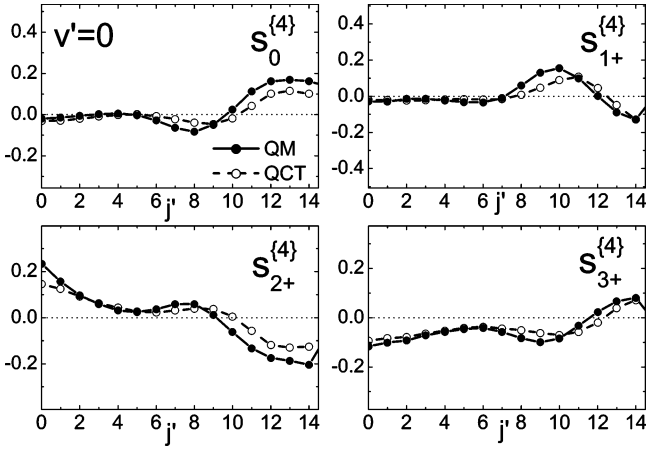

Figure 6. As in Figure 5, but with $k = 4$ and $q = 0-3$.

stereodynamical portraits of reactions leading to HD($j' = 5$) or HD($j' = 10$) (see Figure 3). The $s_0^{\{2\}}$ parameter is the one whose value changes the most between $j' = 5$ and $j' = 10$, going from rather negative at $j' = 5$ (its quantum value is -0.18, whereas the negative limit[18] for $j = 2$ is -0.53) to rather positive at $j' = 10$ (its quantum value is 0.16, whereas the positive limit[18] for $j = 2$ is $+0.53$). Because moments with $k = 2$ and $q = 0$ are indicative of the alignment of the rotational angular momentum vector with respect to the quantization axis, *z*, the observation that the $s_0^{\{2\}}$ parameter is so important for the reaction dynamics strongly suggests that experiments involving reactant rotational alignment are likely to shed considerable light on the reaction dynamics. The possible experiment we described in Section 4 is precisely of this kind, and we will further explore the impact of reactant rotational alignment on measurable quantities.

Figure 7 shows the intrinsic renormalized PDDCSs of rank $k = 2$ and component $q = 0$ as a function of the scattering angle for selected HD($v' = 0$, j') product states. Before commenting on these results, one must remember that these renormalized PDDCCs are not indicative of reaction probability but rather of the preferred reactant polarization at each scattering angle. Because the reaction probability itself does change with scattering angle, one must take the product angular distributions into account when analyzing the renormalized PDDCSs.

Formation of HD($v' = 0$, $j' = 1$) is dominated by backward scattering, but there is also significant forward scattering. Consideration of Figure 7 shows that the agreement between quantum and quasiclassical data, although quite good in the backward scattering region, is not so good in the forward scattering region, where the QCT calculations fail to reproduce the pronounced oscillations of the quantum PDDCS. This information is interesting, and suggests a purely quantum origin for the observed oscillation, which is also seen in the stereodynamical portraits of Figure 4. One might, for instance, attribute the oscillation to an interference effect, similar to that found by Althorpe and co-workers[62,63] in their plane wave-packet analysis of this reaction; the interference might be between near-side and far-side reaction mechanisms.[64]

In the case of the other product states included in Figure 7, the dynamics is dominated by forward and/or sideways scattering. In these regions, the agreement between quantum and quasiclassical data is generally good, although not as quantitative as the one found for the polarization parameters. As one might expect, the more detailed reaction properties (the PDDCSs) constitute a more stringent test of the accuracy of the calculations than the less detailed ones (the PPs).

Exam of the intrinsic reactant PDDCSs and θ-dependent stereodynamical portraits raises an intriguing question: why does the stereochemistry change so much, and in not such a simple fashion, with the scattering angle? (Here we are not talking about the fast quantum oscillations discussed above but rather about the broader ones that are seen in the quasiclassical as well as in the quantum data.) Here one might, for instance, speculate that the observed changes are related to the characteristics of the "bottleneck" states of the collision complex in the transition-state region. Yet another example of how intrinsic stereodynamical properties can give insight and be relevant for the understanding of reaction mechanisms but also yet another question we shall not consider in this paper.

5.2. The Practical Approach: Experimental Control Possibilities. In Section 5.1, we have only examined intrinsic stereodynamical properties obtained without consideration of actual reactant polarizations. Although that method can give understanding and insight into the reaction stereodynamics, it cannot predict the outcome of practical situations and actual experiments. To deal with these, one needs the practical approach we now describe.

The "practical approach" is largely a trial-and-error procedure, in which reaction outcomes are determined with different reactant polarizations, and the corresponding results are com-

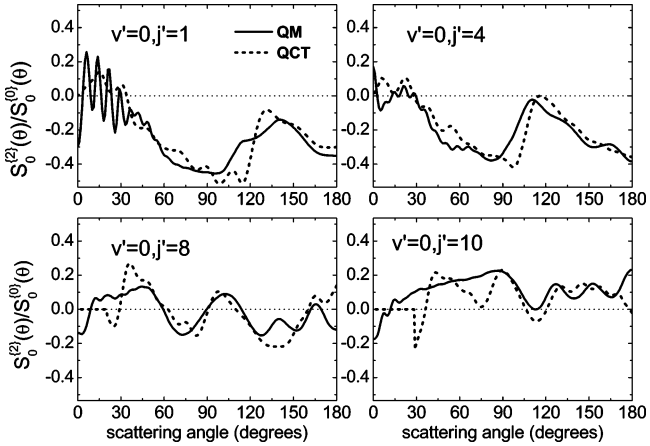

Figure 7. Intrinsic renormalized PDDCSs of rank $k = 2$ and component $q = 0$ of reaction 46 into $v' = 0$, $j' = 1$, 4, 8, or 10 at $E_{coll} = 1.306$ eV as a function of scattering angle.

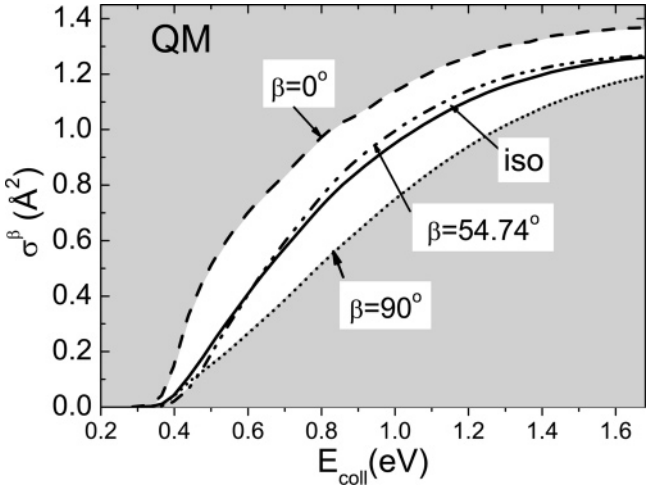

Figure 8. Excitation function of the H + D_2($v = 0$, $j = 2$) reaction for different D_2 alignment directions. The curve labeled as iso corresponds to the situation in which D_2 is unpolarized and the initial **j** vector is therefore random. The borders between the white and gray areas represent the maximum and minimum possible values of σ^{β} and were obtained with the min-maximization procedure described in Section 5.3.

pared. The idea is to examine the extent to which the reaction outcome (say, its cross section or the product state distribution) can be influenced by actual reactant polarization schemes and the extent to which one can use reactant polarization to (passively) control the reaction.

As described in Section 4, the proposed experiment involves D_2 alignment with regard to the reactant-approach direction **k** and possibly the product-recoil direction as well. With this in mind, we have restricted our examples to alignment effects. It should be noted, however, that this is not a necessary restriction; we could have easily included orientation effects in our theoretical examples.

In the experiment we have proposed, the alignment direction is determined by β and α, the polar and azimuthal angles specifying the direction of the electric field vector in *xyz* (the scattering frame of reference, see Sections 2.1 and 4). We consider here cases in which both of these angles are specified (this is appropriate for experiments involving angularly resolved product detection and therefore for measurements of DCSs and special ICSs), and also cases in which only β is determined, whereas α is averaged out (this is appropriate for measurements of ordinary ICSs).

The values we have considered for the polar angle are

$$\beta = 0°,\ 54.74°\ \text{or}\ 90°$$

($\beta = 54.74°$ is the so-called "magic angle" at which $P_2(\cos\beta) = 0$.) When considering specific values for the azimuthal angle, we have used

$$\alpha = 0°,\ 45°,\ 90°\ \text{or}\ 180°$$

When analyzing the data presented below, it will be useful to remember that the D_2 interatomic axis, **r**, and rotational angular momentum, **j**, are respectively aligned along or perpendicular to the direction specified by β and α.

Figure 8 shows quantum data illustrating the effect of the polar angle, β, on the excitation function (the integral cross section, σ^{β}, summed over all product states, as a function of energy). The solid line corresponds to the usual excitation function (isotropic case, no D_2 polarization), whereas the others include the effect of D_2 alignment. The dependence of the

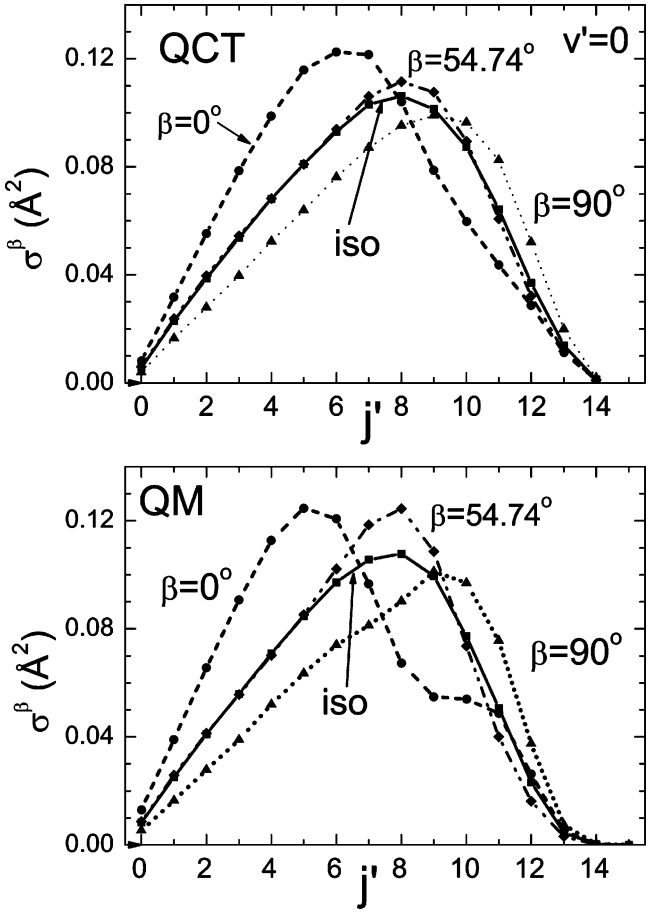

Figure 9. Integral cross section of reaction 47 at $E_{coll} = 1.306$ eV as a function of the product rotational state for different D_2 alignment directions. The top panel shows quasiclassical results, and the bottom panel shows quantum mechanical ones.

reaction cross section on the reactant alignment is clear: reactivity is enhanced by head-on collinear collisions ($\beta = 0°$, **r** parallel to **k** and **j** perpendicular to **k**), diminished by side-on collisions ($\beta = 90°$, **r** perpendicular to **k** and **j** parallel to **k**), and largely unaffected by alignment along the magic angle (which is equivalent to using equal amounts of collinear and perpendicular alignment). Although this is not exactly an unexpected result for the reaction we are considering here (the H + D_2 reaction has long been known to be collinearly-constrained), one should note that Figure 8, besides revealing a preference for collinear collisions, also *quantifies* it, showing the extent to which the reactivity can be controlled by selective reactant polarization.

The effect of D_2 alignment on product rotational state distributions at $E_{coll} = 1.306$ eV (the HD vibrational state is $v' = 0$) is clearly seen in Figure 9, which shows quasiclassical (top) and quantum (bottom) data, obtained with the same β values considered above. The two data sets are in very good agreement, indicating a clear effect: collinear collisions ($\beta = 0°$) lead to a colder product rotational state distribution, whereas side-on collisions ($\beta = 90°$) make it hotter, and magic-angle alignment again leads to results similar to those obtained without reactant polarization. Consideration of these results, along with the stereodynamical portraits of Figure 3, suggests that low/high j' values are associated with collision with low/high impact parameters and thus with transition states with lower/higher bending vibrational energy. Note that the integral cross sections for formation of the product states considered in Figure 3, $j' =$

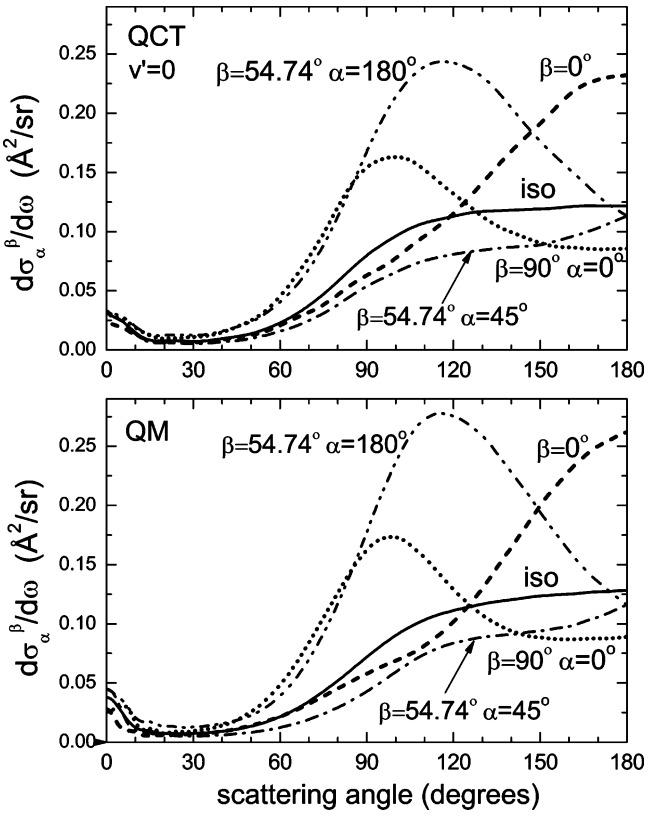

Figure 10. Differential cross section, summed over product rotational states, of reaction 47 at $E_{coll} = 1.306$ eV and for different D_2 alignment directions. The top panel shows quasiclassical results, and the bottom panel shows quantum mechanical ones.

5 and 10, respond to reactant alignment in opposite ways, with one being enhanced when the other is diminished.

Comparison of the rotational distributions of Figure 9 with the polarization parameters of Figures 5 and 6 is also illustrative. The first thing to note is that, because the product recoil direction is not specified, we have cylindrical symmetry around the reactant-approach direction, **k**: as shown by eqs 15 and 43, the only polarization parameters that contribute to the integral cross section are $s_0^{\{0\}}$, $s_0^{\{2\}}$, and $s_0^{\{4\}}$; of these, $s_0^{\{2\}}$ is the one that is largely responsible for the polarization effects (see Section 5.1). As shown in Figure 5, this PP is quite negative for $j' \lesssim 5$ and quite positive for $j' \gtrsim 10$, changing sign around $j' = 8$. No surprise, then, that preparation of reactants with $a_0^{\{2\}} = -0.535$, 0, or 0.267 (these are the quantum values of the extrinsic polarization moments corresponding to reactant alignment along $\beta = 0$, 54.74, or 90°, respectively) lead to increasingly hot product rotational state distributions.

We now turn to the effect of reactant polarization on differential cross sections, which requires us to also consider specific values for the azimuthal angle, α. This further increases the stereospecificity of the experiment and can have a dramatic effect on the ability to control the system reactivity.

Figure 10 shows quasiclassical (top) and quantum (bottom) differential cross sections for reactions leading to HD($v' = 0$, $j' =$ all) at $E_{coll} = 1.306$ eV, considering selected combinations of values for β and α as well as reactions without reactant polarization (labeled as "iso" in the picture). Given the level of detail of the property being considered, the agreement between quantum and QCT data is indeed remarkable, as is the variety of shapes one can obtain for the angular distributions by varying the direction along which the reactant molecule is aligned (i.e., by selecting specific values for β and α).

Inspection of Figure 10 shows that head-on collisions (those favored by $\beta = 0°$) lead to an angular distribution that, compared to the one obtained in the isotropic case (that is, when the collision involves unpolarized reactants), is more focused on the backward scattering region. However, side-on collisions (those favored by $\beta = 90°$) enhance sideways scattering, whereas alignment along the magic angle ($\beta = 54.74°$) leads to an intermediate result.

Also quite evident in Figure 10 is the importance of the azimuthal angle, α, whose value can have a dramatic effect on the observed results. This is illustrated by the curves obtained with $\beta = 54.74°$, $\alpha = 45°$ or with $\beta = 54.74°$, $\alpha = 180°$: although the former polarization direction leads to a DCS that has a similar shape to but is less intense than the DCS obtained with isotropic reactants, the latter leads to a very significant enhancement of the DCS, which is particularly pronounced near $\theta = 115°$. Note that $\alpha = 0°$ and $\alpha = 180°$ both correspond to situations in which the internuclear axis is on or near the scattering plane containing **k** and **k′**, but that the respective collision geometries differ, with the D_2 interatomic axis being tilted along the quadrants of the scattering frame where the $r_x r_z$ product is either negative or positive. Values of α in the $45° \leq \alpha \leq 135°$ range, however, indicate the predominance of collisions in which the D_2 interatomic axis is close to perpendicular to the scattering plane. The fact that a large increase in the DCS is observed for $\alpha = 180°$ indicates that the reaction is predominantly coplanar; that is, the scattering plane and that containing the three atoms remain coincident in the course of the reaction.

We present further illustration of the importance of the azimuthal angle, α, for the observed differential cross section in Figure 11. It contains quantum state-to-state results for reactions leading to HD($v' = 0$, $j' = 0$) scattering in the backward (top) and forward (bottom) scattering regions (the DCS of such reactions in the $30° \leq \theta \leq 120°$ region is invariably very small); the combinations of β and α values are the same ones used in Figure 10. Besides confirming the sensitivity of the product angular distribution to the value of the azimuthal angle, α, Figure 11 shows that the variation can be significant even within strikingly small scattering angle intervals (something that, from the point of view of intrinsic properties, was illustrated by the strongly contrasting stereodynamical portraits of Figure 4). Let us compare, for instance, $\beta = 0°$ to $\beta = 54.74°$, $\alpha = 180°$: the first polarization direction leads to DCS maxima at $\theta = 0°$ and $\theta = 180°$ and to scattering nodes near $\theta = 6°$ and $\theta = 160°$, whereas the second polarization direction leads to a DCS with scattering nodes where the first had maxima and with local maxima where the first had nodes. In our opinion, it is truly remarkable that such contrasts can be observed within such small scattering angle intervals.

Another way of visualizing the effect of the D_2 alignment direction on the reaction we are considering here is by using scattering angle-recoil velocity polar maps such as the ones in Figure 12, which were plotted using quantum data obtained with $E_{coll} = 1.306$ eV. These polar maps show the value of the DCS over a plane in which the polar angle represents the scattering angle, θ, whereas the radial distance to the center is a measure of the product recoil energy (the larger the distance the larger the recoil energy and the smaller the internal energy of the products; the outer ring corresponds to $v' = 0$, $j' = 0$, and v' and j' increase toward the center). Previous observations are also visible in these plots: collinear collisions (D_2 alignment along $\beta = 0°$) lead to a pronounced enhancement of backward

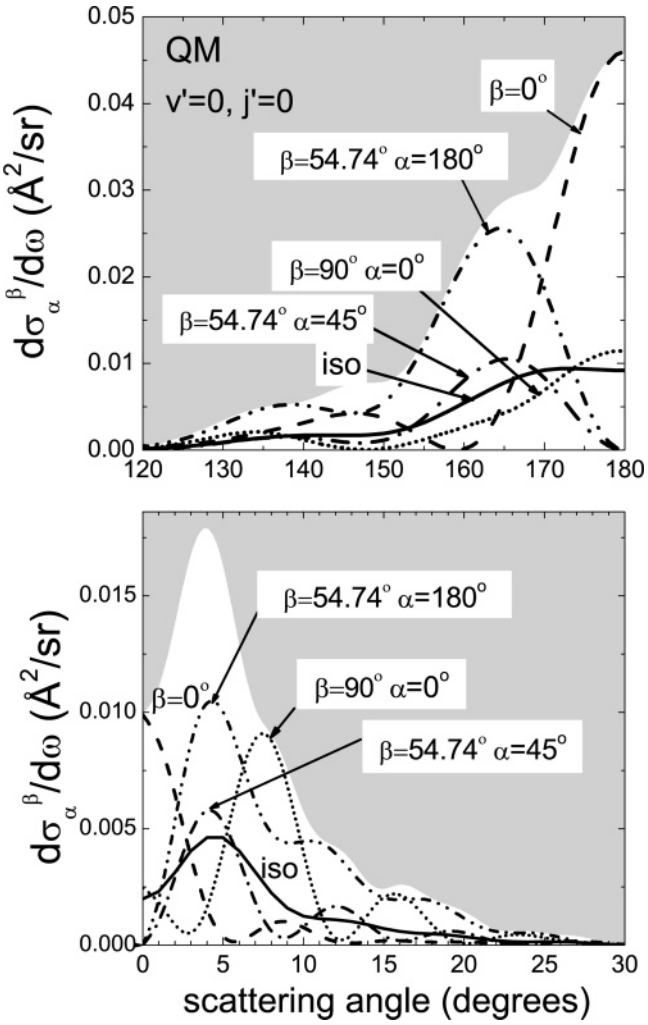

Figure 11. Quantum differential cross section of reaction 48 at E_{coll} = 1.306 eV and for different D_2 alignment directions. The top and bottom panel show the backward and forward scattering region, respectively. The border between the white and gray areas represents the maximum possible values of $d\sigma_\alpha^\beta/d\omega$. The minimum possible values lie at the horizontal, $d\sigma_\alpha^\beta/d\omega = 0$ axis. The minimum and maximum values were obtained with the min-maximization procedure described in Section 5.3.

scattering with regard to the isotropic case (no D_2 polarization), whereas side-on collisions ($45° \leq \beta \leq 135°$) lead to an enhancement of sideways scattering, with the shapes and magnitudes of the polar maps also depending on whether the side-on collisions are coplanar or not. It also becomes clear from these representations that side-on collisions give rise to an appreciable rotational excitation especially manifest in the sideways scattering.

Another example of the effect of the D_2 alignment on the reactivity can be obtained as follows: suppose that we integrate each of the previous polar maps over the scattering angle and the recoil velocity. The resulting quantity, the special ICS, obviously depends on both β and α. Note that in this case the position of the scattering plane is well defined with respect to the direction of the polarization vector of the excitation laser despite the integration over the scattering angle, θ. The results obtained as a function of the collision energy are represented in Figure 13 for different combinations of β and α. As will be explained in Section 5.3, the magnitude of the special ICS is bound within the range indicated by the white area of the figure for a laboratory preparation of $|j = 2, m = 0\rangle$. At low collision energies, the highest and lowest values of $\tilde{\sigma}_\alpha^\beta$ are obtained with $\beta = 0°$ and with $\beta = 90°$, $\alpha = 0°$, respectively. However, with increasing E_{coll}, the alignments that maximize and minimize the special ICS tend to be those with β equal to the magic angle and $\alpha = 180°$ and $\alpha = 0°$, respectively. This indicates that side-on attack with the internuclear axis in the scattering plane can lead to maximal as well as minimal values for the special ICS, depending on the value of α. This azimuthal angle is thus shown to be a very relevant stereodynamical parameter.

5.3. The Min-Max Approach: Theoretical Control Limits. The results we have just presented show that D_2 polarization, and D_2 alignment in particular, can have a dramatic effect on the outcome of the H + D_2 collision. By selecting specific directions for the D_2 alignment, we have obtained starkly contrasting reactive cross sections as well as starkly contrasting product state distributions.

The question that follows is this: is it possible to improve on those results? Can one make the contrasts even starker? If one wants to, say, increase or decrease the reactive cross sections, how far can one go? This is where the min-max approach steps in.

In other words, the question asked in the previous paragraph was, "can one determine the (extrinsic) reactant polarization moments that lead to minimal and maximal reactive cross sections?" The answer is that this is not only possible, but (theoretically at least) rather straightforward. All one has to do is, having determined intrinsic PPs and PDDCSs, to apply standard computational minimization/maximization techniques[69] using the cross section formulas. (In the most general case, these are eqs 8, 14, and 15. If the goal is to determine what is achievable with the experimental setup described above, then the required formulas are those of eqs 41−43.) We have done that and have found that the calculations invariably converge promptly.

Results from two such "min-max" calculations are shown in Figures 8 and 13. In these two cases, we were interested in the determination of the direction of $D_2(v = 0, j = 2)$ alignment that would lead to the largest or smallest possible values for the ICS (Figure 8) or for the special ICS (Figure 13).

In the case of the ICSs of Figure 8, the only adjustable parameter is the angle β, see eq 43. Its determination has led to the minimal and maximal ICSs depicted in Figure 8 as the borders between the theoretically allowed (white) and theoretically forbidden (gray) regions for σ^β. Figure 14 further illustrates the results obtained, showing on its left panel the β values leading to minimal and maximal ICSs at the collision energies considered; note that because the azimuthal angle, α, plays no role here (it is averaged out, as discussed in Sections 2.8 and 4), one does not need to consider β values outside the $0 \leq \beta \leq 90°$ range.

Figure 14 shows that the β values that maximize σ^β are invariably close to zero. This explains why the $\beta = 0°$ curve is invariably at or very close to the upper limit of the allowed σ^β region in Figure 8 and is further evidence that collinear H + D_2 collisions lead to an increased reactivity, although we will have more to say about this in the next paragraph. As for the β values that minimize σ^β, they are invariably close to $\beta = 90°$. This explains why the $\beta = 90°$ curve is invariably at or very close to the lower limit of the allowed σ^β region in Figure 8, and complements the maximization information, showing that side-on H + D_2 collisions lead to a decreased reactivity.

Min-maximization of the special ICS of Figure 13 involves two adjustable parameters (β and α) rather than only one, see eq 42. Their determination has led to the minimal and maximal special ICSs depicted in Figure 13 as the borders between the

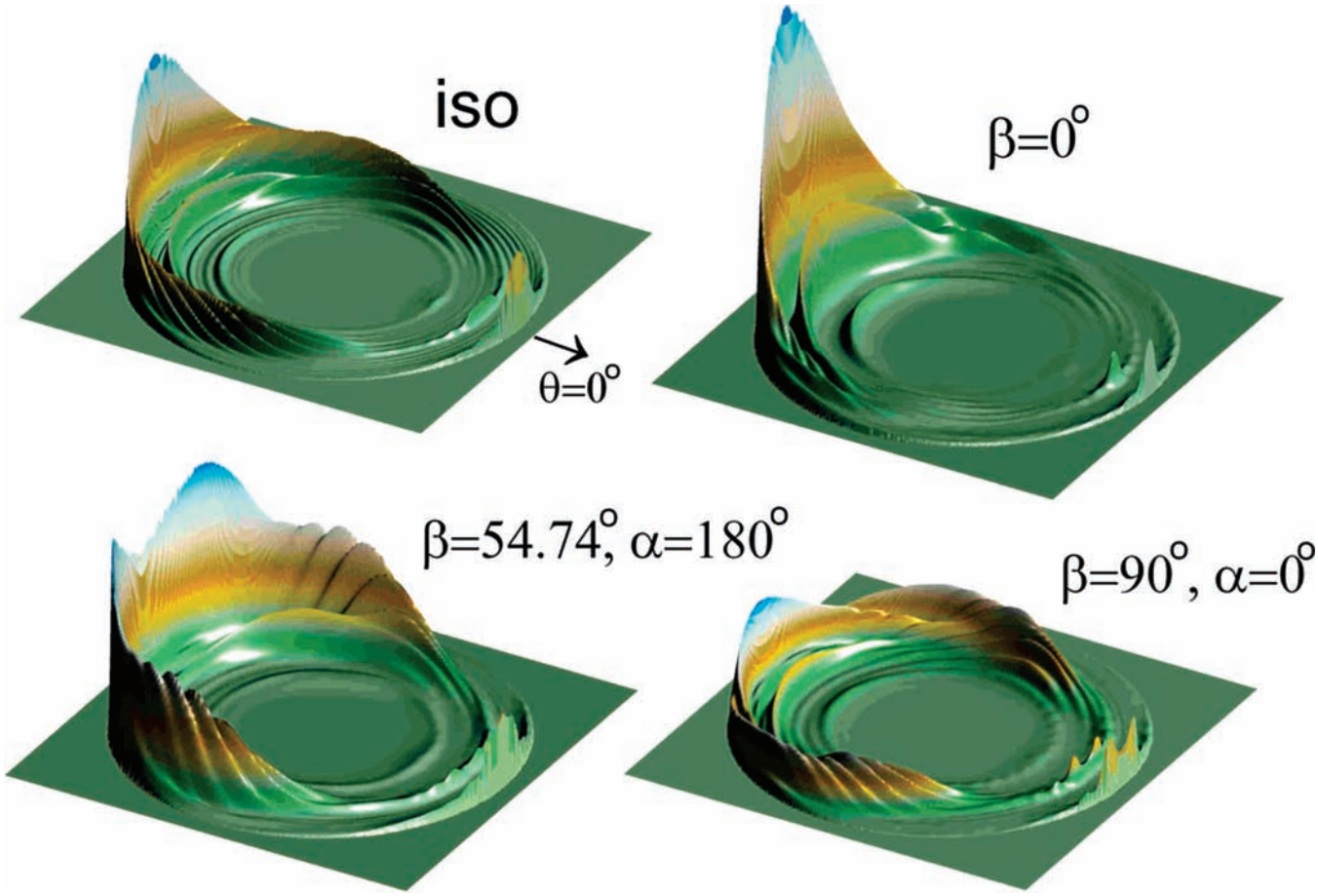

Figure 12. Quantum triple (angle-velocity) differential cross section of the H + D_2 reaction at E_{coll} = 1.306 eV and for different D_2 alignment directions.

theoretically allowed (white) and theoretically forbidden (gray) regions for σ_{α}^{β}. Figure 14 again further illustrates the results obtained, showing on its right panel the β and α values leading to minimal and maximal special ICSs at the collision energies considered.

Figure 14 shows that the β and α values that maximize $\tilde{\sigma}_{\alpha}^{\beta}$ satisfy $\beta < 90°$, $\alpha = 180°$: reactivity is enhanced by coplanar collisions in which the D_2 interatomic axis is tilted toward the incoming H atom rather than away from it. It also shows that, when a more detailed analysis is carried out, one finds that, as far as reactivity is concerned, the best collision geometry is actually not collinear. Indeed, none of our $\tilde{\sigma}_{\alpha}^{\beta}$ maximizations have led to zero as the optimum β value. Instead, we have found that this optimum value steadily increases from $\beta \approx 15°$ near the reaction threshold to $\beta \approx 60°$ at the highest collision energies considered. At the high collision energies, the optimum collision geometry is not even approximately collinear as suggested by the σ^{β} values, but rather coplanar and approximately side-on. This explains why the $\beta = 0°$ curve is close to the upper limit of the allowed $\tilde{\sigma}_{\alpha}^{\beta}$ region in Figure 13 only at very low collision energies and also why at higher collision energies it is coplanar magic-angle collisions that lead to special ICSs approaching their maximum possible values. As shown by Figure 13, selection of the azimuthal angle allows one to double the system reactivity.

As for the β and α values that minimize $\tilde{\sigma}_{\alpha}^{\beta}$, they invariably indicate that side-on collisions in which the D_2 axis is perpendicular to the scattering plane are those that reduce reactivity the most. Consideration of Figure 13, however, leads to an interesting observation: coplanar magic-angle collisions in which the D_2 interatomic axis is tilted the "wrong" way (away from the incoming H atom rather than toward it) can lead to a similar reactivity reduction, in particular at the higher collision energies at which the "right" coplanar magic-angle collisions lead to almost maximum $\tilde{\sigma}_{\alpha}^{\beta}$ values.

We close this section with three remarks about application of the min-max approach. The first is that, although the min-max calculations we have reported on have been constrained (the scattering-frame extrinsic reactant polarization moments were obtained by rotation of laboratory-frame moments, and the values of these were fixed), they do not have to be limited in this way: the values of the extrinsic reactants polarization moments, the $a_q^{(k)}$ values, can be chosen freely. Unconstrained min-max calculations are not significantly harder than constrained ones, and we have actually performed many of those. (They can lead to significantly larger maximal cross sections and to virtually zero minimal cross sections.) Experimental verification of the unconstrained results, however, is currently unfeasible, although the situation may change when adaptive control experiments of the type pioneered by Gerber and coworkers[70] become able to deal with bimolecular collisions.

The second remark is that, although we have only discussed min-max results for integral cross sections, the approach can also be applied to other reaction properties, for example, differential cross sections and product state distributions. (Indeed, Figure 11 shows min-max results for a differential cross section, the maximization results are shown as the border between the theoretically allowed (white) and theoretically forbidden (gray) regions, whereas the minimization results

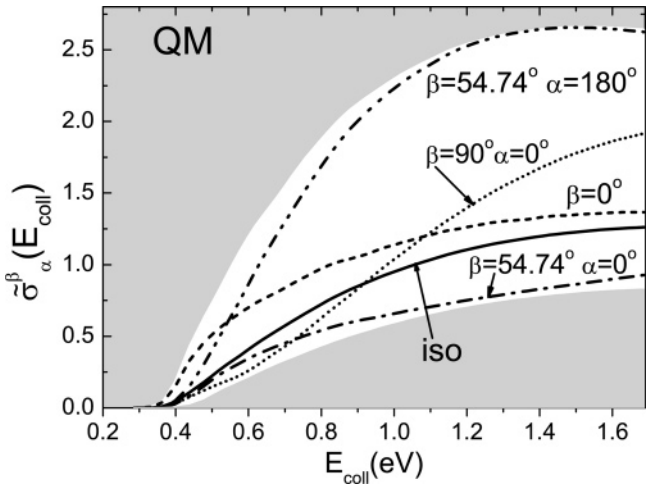

Figure 13. Quantum special ICS as a function of the H + D_2 ($v = 0$, $j = 2$) collision energy for different D_2 alignment directions specified by the values of β and α. The borders between the white and gray areas represent the maximum and minimum possible values of $\tilde{\sigma}^{\beta}_{\alpha}$ and were obtained with the min-maximization procedure described in Section 5.3.

(which have lead to a vanishing DCS for every scattering angle) lie along the horizontal, $d\sigma^{\beta}_{\alpha}/d\omega = 0$ axis.)

The final remark is that, in general, the results from min-max calculations will be better represented by extrinsic stereodynamical portraits (or, equivalently, by a complete set of extrinsic polarization moments) than by a single direction along which reactants are to be oriented or aligned. In the case of the results presented above, the distinction was unnecessary because the calculations were done with the experimental setup described in Section 4 in mind and the β and α values uniquely determined the extrinsic reactants portraits and polarization moments, see Figure 1 and eq 40. However, this is not always the case; in unconstrained min-maximizations, for instance, this is certainly not so. In general, it is comparison between the actual (extrinsic) reactants polarization portraits and their intrinsic counterparts that will allow one to obtain the full picture. We can use production of pure states as an example. If we are interested in, say, the DCS of reaction 48 at $E_{coll} = 1.306$ eV and $\theta = 4°$, we know what the result of an unconstrained maximization must be: the extrinsic reactants portraits must be identical to the intrinsic portraits shown in the top row of Figure 4. This is because in the case of production of pure states it is possible to create a pure reactant polarization state that, in terms of the metaphor introduced earlier, gives to the reaction exactly what it wants. Considering the stereodynamical portraits in Figure 4, one can see that they are not defined simply by a particular direction in space because their shapes can also change. To fully understand the stereochemistry of a reactive collision, one must consider the full picture (directions *and* shapes of the spatial distributions of molecular axes and rotational angular momenta) rather than a single spatial direction.

6. Conclusions

Motivated by the possibility that such work might contribute to an increased understanding of molecular collisions and to a better assessment of experimental control possibilities, we have presented a theoretical method and proposed an experiment for the study of the effect of the reactants polarization on the dynamics of atom−diatom collisions.

The theoretical formalism was stated in general terms. This allows it to deal with arbitrary reactant polarization schemes,

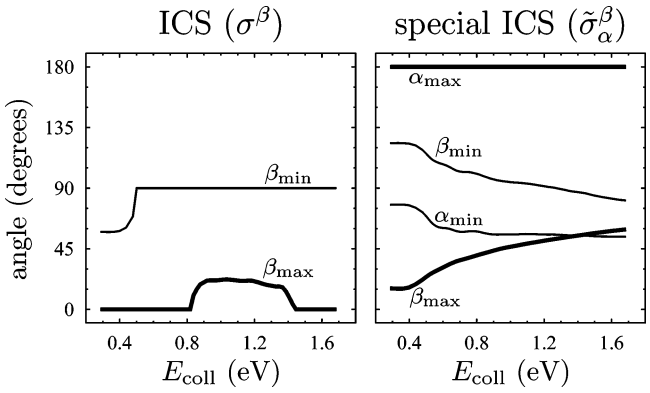

Figure 14. Values of the angles specifying the D_2($v = 0$, $j = 2$) alignment directions leading to maximal or minimal ICSs and special ICSs according to QM. The maximal and minimal ICSs are shown in Figure 8, and the maximal and minimal special ICSs in Figure 13. In either case, they appear in those figures as the borders between the theoretically allowed (white) and theoretically forbidden (gray) regions.

and to be used in conjunction with both quantum reactive scattering and quasiclassical trajectory calculations.

In terms of understanding, two central aspects of the theory presented here are (i) the formal distinction between and separation of intrinsic and extrinsic reactant polarizations, and (ii) the introduction of stereodynamical portraits.

The separation of intrinsic reactant polarizations from their extrinsic counterparts allows one to analyze the collision stereodynamics per se, without consideration of external factors that, although indispensable in practical situations, can be restrictive with regard to analyses of reaction mechanisms. That does not imply, however, that extrinsic polarizations and practical situations cannot be considered: they can, and have been, in a straightforward and flexible way.

The introduction of stereodynamical portraits allows for a visual description of reaction stereodynamics that, although not containing more information than the traditional one in terms of polarization moments only, conveys that information in what we think is a very informative and intuitively appealing way. The need for such visual representations has long been recognized, at least since 1990, when Levine[61] introduced the concept of chemical shape of colliding molecules, but in our opinion the potential of the idea had not yet been fully realized. The reason was the lack of an exact way of graphically representing angular momentum distributions, a problem that has only been solved recently.[46,47]

In terms of experimental control possibilities, we think that the main contribution of this article is the description of an experiment that, although seriously challenging, should be feasible with current technology. Successful conduction of this experiment would allow for stringent tests of the theoretical predictions.

We have used quantum and quasiclassical results for the benchmark H + D_2 reaction to illustrate how the theoretical methods can be used and what can be achieved in the proposed experiment. In so doing, we have found that D_2 polarization, and alignment in particular, has (theoretically at least) a large influence on reaction cross sections and product state distributions.

Some of the results we have obtained reveal not only strong but also surprising effects. A representative example in that regard is the observation that, when the collision energy exceeds 1 eV, the collision geometry that maximizes the cross section of the "collinearly constrained" H + D_2 reaction is actually not collinear at all. Instead, it is side-on, with strong coplanarity

requirements. Although the "right" type of coplanar side-on collision leads to maximal reactivity, the "wrong" one takes reactivity very close to its lowest possible value.

In the introduction to this paper, using the Li + HF system as an example, we have commented on how detailed studies of the stereodynamics of molecular collisions often lead to unexpected results. This has also proved to be the case for H + D_2, by far the most studied and best understood of all elementary reactions. This shows that much remains to be done if we are to thoroughly understand the influence of stereochemical factors on the reactivity of such systems. More research is necessary, and we hope the results reported here will help motivate experimentalists and theoreticians alike to further work on this beautiful and intriguing problem.

Acknowledgment. We wish to dedicate this article to Professor John P. Simons (Oxford University) on his seventieth anniversary. We owe him a great deal of inspiration and encouragement, always accompanied by great doses of humor, for continuing our work on vector correlations. We also thank Greg Sitz and Dionisio Bermejo for their insightful comments on the feasibility of the proposed experiment. J.A. acknowledges financial support by a FPU fellowship of the Spanish Ministry of Education and Science and by grant BQU2002-04462-C02-01. F.J.A. and V.S.R. acknowledge funding by the Spanish Ministry of Education and Science under grant BQU2002-04627-C02. B.K.K. acknowledges that part of this work was done under the auspices of the U.S. Department of Energy under Project no. 20020015ER of the Laboratory Directed Research and Development program at Los Alamos under Contract no. W-7405-ENG-36.

References and Notes

(1) Simons, J. P. *Faraday Discuss.* **1999**, *113*, 1.
(2) Levine, R. D.; Bernstein, R. B. *Molecular Reaction Dynamics and Chemical Reactivity*; Oxford University Press: Oxford, U.K., 1987.
(3) Alexander, A. J.; Zare, R. N. *J. Chem. Educ.* **1998**, *75*, 1105.
(4) Houston, P. L. *J. Phys. Chem.* **1996**, *100*, 12757.
(5) Bernstein, R. B.; Levine, R. D.; Herschbach, D. R. *J. Phys. Chem.* **1987**, *91*, 5365.
(6) Rice, S. A.; Zhao, M. *Optical Control of Molecular Dynamics*; Wiley: New York, 2000.
(7) Gordon, R. J.; Rice, S. A. *Annu. Rev. Phys. Chem.* **1997**, *48*, 601.
(8) Shapiro, M.; Brumer, P. *J. Chem. Soc., Faraday Trans.* **1997**, *93*, 1263.
(9) *Chem. Phys.* **2004**, *301* (Stereodynamics of Molecular Reactions), 159−332.
(10) *Faraday Discuss.* **1999**, *113* (Stereochemistry and Control in Molecular Reaction Dynamics), 1−504.
(11) *J. Phys. Chem. A* **1997**, *101* (Stereodynamics of Chemical Reactions), 7461−7690.
(12) *J. Phys. Chem.* **1995**, *99* (Stereodynamics and Active Control in Chemical Reactions), 13569−13754.
(13) *J. Chem. Soc., Faraday Trans.* **1993**, *89* (Orientation and Polarisation Effects in Chemical Reacion Dynamics), 1401−1592.
(14) *J. Phys. Chem.* **1991**, *95* (R. B. Bernstein Memorial Issue on Molecular Dynamics), 7961−8421.
(15) *J. Chem. Soc., Faraday Trans.* **1989**, *85* (Stereodynamics Issue), 925−1376.
(16) *J. Phys. Chem.* **1987**, *91* (Stereodynamics Issue), 5365−5515.
(17) de Miranda, M. P.; Clary, D. C. *J. Chem. Phys.* **1997**, *106*, 4509.
(18) de Miranda, M. P.; Aoiz, F. J.; Bañares, L.; Sáez-Rábanos, V. *J. Chem. Phys.* **1999**, *111*, 5368.
(19) Kandel, S. A.; Alexander, A. J.; Kim, Z. H.; Zare, R. N.; Aoiz, F. J.; Bañares, L.; Castillo, J. F.; Sáez-Rábanos, V. *J. Chem. Phys.* **2000**, *112*, 670.
(20) Orr-Ewing, A. J. *J. Chem. Soc., Faraday Trans.* **1996**, *92*, 881.
(21) Shafer-Ray, N. E.; Orr-Ewing, A. J.; Zare, R. N. *J. Phys. Chem.* **1995**, *99*, 7591.
(22) Orr-Ewing, A. J.; Zare, R. N. *Annu. Rev. Phys. Chem.* **1994**, *45*, 315.
(23) Zare, R. N. *Angular Momentum: Understanding Spatial Aspects in Chemistry and Physics*; Wiley: New York, 1988.
(24) Greene, C. H.; Zare, R. N. *Annu. Rev. Phys. Chem.* **1982**, *33*, 119.
(25) Dixon, R. N. *J. Chem. Phys.* **1986**, *85*, 1866.
(26) Barnwell, J. D.; Loeser, J. G.; Herschbach, D. R. *J. Phys. Chem.* **1983**, *87*, 2781.
(27) Biedenharn, L. C.; Louck, J. D. *Angular Momentum in Quantum Physics: Theory and Application*; Addison-Wesley: Reading, MA, 1981.
(28) Biedenharn, L. C. in *Nuclear Spectroscopy, Part B*; Azjenberg-Selove, F., Ed.; Academic: New York, 1960.
(29) Fano, U.; Racah, G. *Irreducible Tensorial Sets*; Academic: New York, 1959.
(30) Fano, U. *Rev. Mod. Phys.* **1957**, *29*, 74.
(31) Allison, T. C.; Lynch, G. C.; Truhlar, D. G.; Gordon, M. S. *J. Phys. Chem.* **1996**, *100*, 13575.
(32) Alvariño, J. M.; Aquilanti, V.; Cavalli, S.; Crocchianti, S.; Laganà, A.; Martínez, M. T. *J. Phys. Chem. A* **1998**, *102*, 9638.
(33) de Miranda, M. P.; Crocchianti, S.; Laganà, A. *J. Phys. Chem. A* **1999**, *103*, 10776.
(34) Alvariño, J. M.; Basterrechea, F. J.; Laganà, A. *Mol. Phys.* **1986**, *59*, 559.
(35) Loesch, H.-J.; Stienkemeier, F. *J. Chem. Phys.* **1993**, *98*, 9570.
(36) Höbel, O.; Loesch, H.-J. *Faraday Discuss. Chem. Soc.* **1999**, *113*, 337.
(37) Lara, M.; Aguado, A.; Roncero, O.; Paniagua, M. *J. Chem. Phys.* **1998**, *109*, 9391.
(38) Aoiz, F. J.; Martínez, M. T.; Sáez-Rábanos, V. *J. Chem. Phys.* **2001**, *114*, 8880.
(39) Fano, U.; Macek, J. H. *Rev. Mod. Phys.* **1973**, *45*, 553.
(40) Greene, C. H.; Zare, R. N. *J. Chem. Phys.* **1983**, *78*, 6741.
(41) Orr-Ewing, A. J.; Simpson, W. R.; Rakitzis, T. P.; Zare, R. N. *Isr. J. Chem.* **1994**, *34*, 95.
(42) Yan, C.; Kummel, A. C. *J. Chem. Phys.* **1993**, *98*, 6869.
(43) Rutkowski, M.; Zacharias, H. *Chem. Phys.* **2004**, *301*, 189; Rutkowski, M.; Zacharias, H. *Chem. Phys.* **2005**, *310*, 321.
(44) Costen, M. L.; Crichton, H. J.; McKendrick, K. G. *J. Chem. Phys.* **2004**, *120*, 7910.
(45) Costen, M. L.; Hall, G. E. *Phys. Chem. Chem. Phys.* **2005**, *7*, 1408.
(46) de Miranda, M. P.; Aoiz, F. J. *Phys. Rev. Lett.* **2004**, *93*, 083201.
(47) de Miranda, M. P.; Aoiz, F. J.; Sáez-Rábanos, V.; Brouard, M. *J. Chem. Phys.* **2004**, *121*, 9830.
(48) Auzinsh, M.; Ferber, R. *Optical Polarization of Molecules*; Cambridge University Press: Cambridge, U.K., 1995.
(49) Hertell, I. V.; Stoll, W. *Adv. At. Mol. Phys.* **1978**, *13*, 113.
(50) Varshalovich, D. A.; Moskalev, A. N.; Khersonskii, V. K. *Quantum Theory of Angular Momentum*; World Scientific: Singapore, 1988.
(51) Blum, K. *Density Matrix Theory and Applications*, 2nd ed.; Plenum: New York, 1996.
(52) Aoiz, F. J.; Brouard, M.; Enríquez, P. A. *J. Chem. Phys.* **1996**, *105*, 4964.
(53) Althorpe, S. C. *Int. Rev. Phys. Chem.* **2004**, *23*, 219.
(54) Althorpe, S. C. *J. Chem. Phys.* **2004**, *121*, 1175.
(55) Althorpe, S. C. *Phys. Rev. A* **2004**, *69*, 042702.
(56) Althorpe, S. C. *J. Chem. Phys.* **2001**, *1114*, 1601.
(57) Zhang, J. Z. H.; Miller, W. H. *J. Chem. Phys.* **1989**, *91*, 1528.
(58) Boothroyd, A. I.; Keogh, W. J.; Martin, P. G.; Peterson, M. R. *J. Chem. Phys.* **1996**, *104*, 7139.
(59) Kendrick, B. K. *J. Chem. Phys.* **2001**, *114*, 8796.
(60) Aoiz, F. J.; Bañares, L.; D'Mello, M. J.; Herrero, V. J.; Sáez Rábanos, V.; Schnieder, L.; Wyatt, R. E. *J. Chem. Phys.* **1994**, *101*, 5781.
(61) Levine, R. D. *J. Phys. Chem.* **1990**, *94*, 8872.
(62) Althorpe, S. C.; Fernandez-Alonso, F.; Bean, B. D.; Ayers, J. D.; Pomerantz, A. E.; Zare, R. N.; Wrede, E. *Nature* **2002**, *416*, 67.
(63) Althorpe, S. C. *J. Chem. Phys.* **2002**, *117*, 4623.
(64) Noli, C.; Connor, J. N. L.; Rougeau, N.; Kubach, C. *Phys. Chem. Chem. Phys.* **2001**, *3*, 3946.
(65) Sitz, G. O.; Farrow, R. L. *J. Chem. Phys.* **1994**, *101*, 4682.
(66) Code, R. F.; Ramsey, N. F. *Phys. Rev. A* **1971**, *4*, 1945.
(67) Schnieder, L.; Seekamp-Rahn, K.; Wrede, E.; Welge, K. H. *J. Chem. Phys.* **1997**, *107*, 6175.
(68) Harich, S. A.; Dai, D.; Wang, C. C.; Yang, X.; Chao, S. D.; Skodje, R. *Nature* **2002**, *419*, 281.
(69) Press, W. H.; Teukolsky, S. A.; Vetterling, W. T.; Flannery, B. P. *Numerical Recipes in Fortran 77*; Cambridge University Press: Cambridge, U.K., 1992.
(70) Brixner, T.; Gerber, G. *Chem. Phys. Chem.* **2003**, *4*, 418.